NASA
Technical
Paper
2707

July 1987

Multiscale Turbulence Effects in Supersonic Jets Exhausting Into Still Air

Khaled S. Abdol-Hamid
and Richard G. Wilmoth

NASA

NASA Technical Paper 2707

1987

Multiscale Turbulence Effects in Supersonic Jets Exhausting Into Still Air

Khaled S. Abdol-Hamid
Analytical Services and Materials, Inc.
Hampton, Virginia

Richard G. Wilmoth
Langley Research Center
Hampton, Virginia

National Aeronautics and Space Administration

Scientific and Technical Information Office

Summary

A modified version of the multiscale turbulence model of Hanjalic has been applied to the problem of supersonic jets exhausting into still air. In particular, the problem of shock-cell decay through turbulent interaction with the mixing layer has been studied for both mildly interacting and strongly resonant jet conditions. The modified Hanjalic model takes into account the nonequilibrium energy transfer between two different turbulent spectral scales. The turbulence model was incorporated into an existing shock-capturing, parabolized Navier-Stokes computational model in order to perform numerical experiments.

The results show that the two-scale turbulence model provides significant improvement over one-scale models in the prediction of plume shock structure for underexpanded supersonic (Mach 2) and sonic (Mach 1) jets. For the supersonic jet, excellent agreement with experiment was obtained for the centerline shock-cell pressure decay up to 40 jet radii. For the sonic jet, the agreement with experiment was not as good, but the two-scale model still showed significant improvement over the one-scale model. It is shown that by relating some of the coefficients in the turbulent-transport equations to the relative time scale for transfer of energy between scales, the two-scale model can provide predictions that bound the measured shock-cell decay rate for the sonic jet.

Introduction

Over the last several years, significant progress has been made toward developing an understanding of and a predictive capability for the dominant physical processes in turbulent supersonic jets. Advances in computational fluid dynamics have produced numerical models, such as the SCIPVIS code of Dash and Wolf (ref. 1), which can quantitatively predict many of the details of the shock-cell structure, the turbulent mixing with an external stream, and the subsequent decay of the shock-cell strength as the result of shock/mixing-layer interactions. The fundamental understanding of such phenomena has been enhanced through the development of analytical models such as that of Tam, Jackson, and Seiner (ref. 2), which is based on a linear solution for the shock-cell structure that uses the method of multiple-scale asymptotic expansions. Although the numerical models are generally more useful for quantitative predictions, particularly for nonlinear problems, the analytical wave models can more readily provide information on the spectral components of the flow field. Both models have proven to be useful for predictions related to broadband shock noise (refs. 2 to 4) for mildly underexpanded and mildly overexpanded plumes. The SCIPVIS code can also give accurate predictions of the near-field plume shock structure for highly underexpanded and highly overexpanded cases so long as the flow field is dominated by inviscid processes.

However, for situations in which strong interactions between the shock structure and large-scale turbulent structure are suspected to occur (refs. 2 and 3), neither model adequately predicts the shock-cell decay. In such situations, the relative wavelengths of the turbulent and inviscid structures are such that acoustically stimulated production of large-scale structures is believed to occur and the plume decays or collapses rapidly after a few shock cells. The turbulent processes are in some ways similar to the breakup frequently observed in low-speed jets and shear layers that results from the instability of the flow. In each case, a mechanism for the transfer of energy between different scales of turbulence is required to explain the phenomenon.

The numerical model of reference 1 and the analytical model of reference 2 use turbulence models that are based on the assumption that there is a spectral distribution of turbulent eddies that remains in equilibrium. For the equilibrium assumption to hold, the time scales for the transfer of energy between different turbulence scales must be much different than the time scales associated with the overall production and dissipation of turbulence. In such cases, only a single spectral scale need be considered, because the spectral distribution does not change over the time scale of interest. However, when these time scales are not greatly different, it appears that some modeling of multiscale turbulence effects is needed.

Hanjalic, Launder, and Schiestel (ref. 5) proposed a turbulence closure scheme employing two or more independently calculated time scales to describe the rates of different turbulent interactions. The model was tested with relatively good success for several classes of boundary-layer, free-shear, and jet-mixing problems. Chen (refs. 6 and 7) adapted the model to the problems of confined swirling-jet and recirculating flows with good results. The Hanjalic model adapted by Chen follows the transport formulation of references 8 and 9, with the addition of new equations to describe the transfer of energy between the two scales. Wilcox (ref. 10) has proposed a two-scale closure model which decomposes the Reynolds stress tensor into "large" and "small" eddies and has applied the model with good success to several boundary-layer and shear-flow problems. Each of these models appears to have some merit when studying problems for which a multiscale spectrum of turbulence is expected to be important. However, the Hanjalic model adapted by Chen appears

to be somewhat simpler to implement in numerical jet models such as the SCIPVIS code.

In the present paper, the multiscale turbulence model of Hanjalic is applied to the problem of supersonic jets exhausting into still air. In particular, the problem of shock-cell decay through turbulent interaction with the mixing layer is addressed for both mildly interacting and strongly resonant jet conditions. A typical flow field for an underexpanded, shock-containing, supersonic jet plume is shown in figure 1. The Hanjalic model was incorporated into the SCIPVIS code so that numerical experiments could be performed. The approach was to formulate a two-scale set of parabolized turbulent-energy and dissipation-rate transport equations that were essentially identical to the one-scale, two-equation model of references 8 and 9 that was already contained within the SCIPVIS code. This approach required the addition of two new transport equations to describe the transfer of energy between scales. It is similar to the approach of Chen but is applied here to the steady, parabolic flow equations. The computational model was then applied to several experimental test cases from reference 3.

Symbols

A, B	mapping parameters
a, b, c, d	limiting values of k_P, k_T, ε_P, and ε_T outside the mixing layer
$C_\mu, C_{P1}, C_{P2}, C_{T1}, C_{T2}$	turbulence model coefficients
$\mathbf{E}$, $\mathbf{F}$, $\mathbf{G}_f$	vector arrays of conservation variables
$\mathbf{f}$	vector array of dependent variables
$\tilde{f}$	axisymmetric correction parameter for $k\varepsilon 2$ model
g	weak shear-flow correction parameter for $k\varepsilon 2$ model
H	total enthalpy, $h + 1/2Q^2$
h	static enthalpy
J	planar ($J = 0$) or axisymmetric ($J = 1$) flag
K	compressibility correction factor for $k\varepsilon 2$ model
k	turbulent kinetic energy
k_P	turbulent kinetic energy associated with production
k_T	turbulent kinetic energy associated with transfer
M	Mach number
M_e	fully expanded jet Mach number
M_j	nozzle-exit design Mach number
M_τ	turbulence Mach number
$\underline{P}$	production rate of turbulent kinetic energy
P	static pressure
P_a	ambient static pressure in still air
P_j	static pressure in jet at nozzle exit
Q	total velocity
r	transverse distance
r_j	radius of jet at nozzle exit
r_L, r_U	lower and upper mixing-layer boundaries
U	streamwise mean velocity
U_a	streamwise mean velocity in ambient air
$U_{\text{℄}}$	streamwise mean velocity along jet centerline
u, v	instantaneous velocity fluctuations
V	transverse mean velocity
$\overline{v\gamma}$	time-averaged components of Reynolds stress and/or turbulent heat or concentration fluxes
W	turbulent vorticity
x	streamwise distance
α	subsonic ($\alpha = 0$) or supersonic ($\alpha = 1$) parameter
γ	$= u, v, h,$ or ϕ
ε	dissipation rate of turbulent kinetic energy
ε_P	dissipation rate of turbulent kinetic energy for production

ε_T	dissipation rate of turbulent kinetic energy for transfer
η	mapped transverse coordinate
μ	molecular viscosity
μ_{eff}	effective viscosity, $\mu + \mu_t$
μ_t	turbulent viscosity
ξ	mapped streamwise coordinate
ρ	gas mixture density
σ_f	effective Prandtl number
τ_P, τ_T	time constants associated with filling production and transfer tanks
Φ	species mass-fraction parameter
ϕ	instantaneous species mass fraction

Turbulence Models

Most of the numerical models which have been applied to predict the flow and heat transfer in jet-mixing problems are of the finite-difference type. These solve the time-averaged partial differential equations governing the turbulent transport of heat, mass, or species concentration using a finite-difference numerical approach. The equations describing the mean flow-field quantities for turbulent free shear are well known (e.g., see Tennekes and Lumley (ref. 11)). The mean flow equations for steady-state, two-dimensional flows may be expressed as

$$\frac{\partial \rho U r^J}{\partial x} + \frac{\partial \rho V r^J}{\partial r} = 0 \tag{1}$$

for continuity and

$$\frac{\partial \rho U \Gamma r^J}{\partial x} + \frac{\partial \rho V \Gamma r^J}{\partial r} = \frac{\partial}{\partial r} r^J \left(\frac{\mu}{\beta_\Gamma} \frac{\partial \Gamma}{\partial r} - \rho \overline{v\gamma} \right) + S_\Gamma \tag{2}$$

for momentum or energy conservation, where Γ may stand for either of the velocity components (U and V), total enthalpy H, or a species concentration Φ; μ is the molecular viscosity, and β_Γ is the thermal coefficient. The corresponding source term S_Γ is given by

$$\left.\begin{aligned} -S_U &= r^J \frac{\partial P}{\partial x} \\ -S_V &= r^J \frac{\partial P}{\partial r} \\ S_H = S_\Phi &= 0 \end{aligned}\right\} \tag{3}$$

In the preceding equations, $J = 1$ for axisymmetric flows and $J = 0$ for planar flows. The turbulent stresses ($\gamma = u, v$) or turbulent heat or concentration fluxes ($\gamma = h, \phi$) are represented by $\overline{v\gamma}$.

The derivation of equation (2) is based on the assumption that terms involving density and pressure fluctuations can be neglected compared with the turbulent transport terms. This assumption follows Morkovin's hypothesis, that the density fluctuation ρ' has a small effect on turbulence structure if $\rho'/\rho << 1$ and allows the use of an incompressible turbulence model in a compressible flow for $M < 5$ in a boundary layer and for $M < 1$ in a mixing layer (refs. 12 and 13).

To close equations (1) and (2), additional equations must be prescribed to model the turbulence terms, and this is the main purpose of most turbulence models. Most turbulence closure schemes for shear flows follow Boussinesq's eddy-viscosity concept, which assumes that turbulent stresses and heat and concentration fluxes are proportional to the normal gradient in Γ. Thus, the diffusion terms $\overline{v\gamma}$ may be expressed as

$$\left.\begin{aligned} -\rho\overline{uv} &= \mu_t \frac{\partial U}{\partial r} \\ -\rho\overline{v^2} &= 2\mu_t \frac{\partial V}{\partial r} - 2/3\rho k \\ -\rho\overline{vh} &= \frac{\mu_t}{\sigma_H} \frac{\partial H}{\partial r} \\ -\rho\overline{v\Phi} &= \frac{\mu_t}{\sigma_\Phi} \frac{\partial \Phi}{\partial r} \end{aligned}\right\} \tag{4}$$

In general, for $\gamma \neq v$, $-\overline{v\gamma} = \frac{\mu_t}{\beta_\Gamma} \frac{\partial \Gamma}{\partial r}$.

The turbulent viscosity μ_t is not a fluid property. Its value varies from point to point in the flow field and depends on the state of turbulence.

One-Scale Model

The additional closure assumption that is required is a model for μ_t. One of the most widely used models for the distribution of μ_t is the $k\varepsilon$ (two-equation) turbulence model. According to this model,

$$\mu_t = C_\mu \frac{\rho k^2}{\varepsilon} \tag{5}$$

where $\sqrt{k}$ represents the velocity scale for the large-scale turbulent motion, ε is the rate of dissipation of the turbulent kinetic energy, and C_μ is a coefficient to be prescribed. The distributions of k and ε are obtained from the solution of partial differential equations, which have the same form as equation (2),

where

$$\left.\begin{aligned} S_k &= \underline{P} - \rho\varepsilon \\ S_\varepsilon &= (C_{P1}\underline{P} - C_{P2}\varepsilon)\frac{\varepsilon}{k} \end{aligned}\right\} \quad (6)$$

and the turbulent diffusion fluxes are obtained from equations (4) by substituting k or ε for H. The rate of generation of turbulent kinetic energy (production) by the interaction of turbulent stresses with mean velocity gradients is given by

$$\underline{P} = \overline{uv}\frac{\partial U}{\partial r} \quad (7)$$

This model is based on the assumption that the flows considered are fairly close to a spectral equilibrium. Here, only one time scale $\frac{k}{\varepsilon}$ is considered, and the times associated with the transfer of energy between different spectral regions are assumed to be negligible.

In the present paper, the more elaborate $k\varepsilon 2$ turbulence model of Rodi (refs. 14 and 15) is used. The constants and coefficients for this model (from ref. 15) are as follows.

For planar flows,

$$\begin{aligned} C_\mu &= 0.09g(\overline{\underline{P}/\varepsilon}) \\ C_{P2} &= 1.94 \\ C_{P1} &= 1.40 \\ \beta_k &= 1.0 \\ \beta_\varepsilon &= 1.3 \end{aligned}$$

where

$$\overline{\underline{P}/\varepsilon} = \frac{\int_{r_1}^{r_2} \rho\overline{uv}\left(\frac{\underline{P}}{\varepsilon}\right) r^J \, dr}{\int_{r_1}^{r_2} (\rho\overline{uv})\, r^J \, dr}$$

and where the function $g(\underline{P}/\varepsilon)$ is shown in figure 2. The constants and coefficients for axisymmetric flows are the same as for planar flows except for the following:

$$\begin{aligned} C_\mu &= 0.09g(\overline{\underline{P}/\varepsilon}) - 0.0534\tilde{f} \\ C_{P2} &= 1.94 - 0.1336\tilde{f} \end{aligned}$$

where

$$\tilde{f} = 0 \text{ for } r_L > 0$$

$$\tilde{f} = \left|\frac{r_U}{2(U_\ell - U_a)}\left(\frac{dU_\ell}{dx} - \left|\frac{dU_\ell}{dx}\right|\right)\right|^{0.2} \text{ for } r_L = 0$$

Rodi found that C_μ is not a constant value; it varies significantly with the local rate of turbulence production divided by the rate of dissipation. Figure 2 shows Rodi's proposal for the dependence of the function g on $\overline{\underline{P}/\varepsilon}$ (C_μ is proportional to g). This function was derived for thin shear layers based on correlation of experimental data in which $\underline{P}$ was significantly different than ε, and its use has been shown to significantly improve the ability of the model to predict weak shear flows.

A compressibility correction function to improve the calculated results using $k\varepsilon 2$ (incompressible turbulence model) for supersonic jets and shear layers was proposed in reference 16. The compressibility-corrected viscosity is given by

$$\mu_t = K(M_\tau)C_\mu\frac{\rho k^2}{\varepsilon} \quad (8)$$

where $K(M_\tau)$ is the correction function and M_τ, the turbulence velocity-scale Mach number, is defined as $\sqrt{k_{\max}}/a$. In this expression, $k_{\max}$ is the maximum value of k at a given axial location (across the profile) and a is the local speed of sound at the radial location where k is the maximum. Figure 3 shows the variation of $K(M_\tau)$ with respect to M_τ (from ref. 1). Hereinafter, the $k\varepsilon 2$ turbulence model with the compressibility correction function is referred to as $k\varepsilon 2$-cc.

Two-Scale Model

The basis of the approach used to model multispectral turbulence scales is described in detail in references 5 to 7. This two-scale model takes into account the nonequilibrium spectral-energy transfer mechanism. The key to the two-scale model is the recognition that, although the one-scale dissipation and kinetic-energy equations contain both production and dissipation terms, these processes occur in different spectral regions. The turbulent-energy production occurs in the large eddies in the flow, but dissipation phenomena involve primarily the smaller scales.

Essentially, the kinetic energy is divided into three regions: large-scale energy production, intermediate energy transfer, and small-scale dissipation. At high Reynolds numbers, the energy content of the dissipative eddies is negligible. Thus, the turbulent kinetic energy may be divided into two parts: the large-scale production eddies k_P (containing low-wave-number eddies), and the high-wave-number transfer eddies k_T. Energy leaves the low-wave-number (production) region at a rate of ε_P and enters the high-wave-number region at a rate of ε_T. To simplify the modeling procedure, it has been assumed that spectral equilibrium exists between the transfer region and the dissipation region ($\varepsilon = \varepsilon_T$). This assumption results from considering only a single transfer

mechanism between two spectral scales. If more than one production scale and/or multiple transfer regions were considered, the overall dissipation ε would not be in equilibrium with a single transfer region.

The basis for the two-scale model is shown by the tank-and-tube analogy in figure 4. The amount of energy involved in transfer processes (shown as a tank of level k_T) is controlled by the difference in dissipation, $\varepsilon_P - \varepsilon_T$. Production of turbulence $\underline{P}$ feeds the kinetic energy tank that is designated k_P. The level of energy in each tank is represented by k_P (production) and k_T (transfer); ε_P and ε_T are the valve restrictions of the corresponding tanks. Therefore, the time constants associated with filling the production and transfer tanks can be written as:

$$\left.\begin{aligned} \tau_P &= \frac{k_P}{\varepsilon_P} \\ \tau_T &= \frac{k_T}{\varepsilon_T} \end{aligned}\right\} \tag{9}$$

and the time-scale ratio is

$$T = \frac{\tau_T}{\tau_P} = \left(\frac{k_T}{k_P}\right)\left(\frac{\varepsilon_P}{\varepsilon_T}\right) \tag{10}$$

The value of T may be used to represent the relative rate of turbulent-energy transfer between the large-scale (production) region and intermediate-scale (transfer) region.

Following the previously described one-scale model formulation, the distributions of k_P, k_T, ε_P and ε_T are obtained from the solution of partial differential equations, which have the same form as equation (2) with

$$\left.\begin{aligned} S_{k_P} &= \underline{P} - \rho\varepsilon_P \\ S_{k_T} &= \rho(\varepsilon_P - \varepsilon_T) \\ S_{\varepsilon_P} &= \frac{C_{P1}\underline{P} - C_{P2}\rho\varepsilon_P}{\tau_P} \\ S_{\varepsilon_T} &= \frac{\rho}{\tau_2}\left((C_{T1}\varepsilon_P) - (C_{T2}\varepsilon_T)\right) \end{aligned}\right\} \tag{11}$$

The values of the constants and coefficients used for the present calculations and the values used in the original Hanjalic model (ref. 5) and the Chen version of the model (refs. 6 and 7) are listed in table 1. Also, the following relations were used:

$$\left.\begin{aligned} \beta_{k_T} &= \beta_{k_P} = 1 \\ \beta_{\varepsilon_T} &= \beta_{\varepsilon_P} = 1.22 \\ C_{P2} &= C_{P21} + C_{P22}\left(\frac{R-1}{R+1}\right) \\ R &= \frac{k_P}{k_T} \\ C_{P22} &= -0.3 \end{aligned}\right\} \tag{12}$$

These relations were the same as for the previous models except for the compressibility correction $K(M_\tau)$, for which a value of one was used in the previous work. The constants used in the present study closely follow those of Chen but have been modified somewhat such that in the limit, $k_P \rightarrow k_T$ and $\varepsilon_P \rightarrow \varepsilon_T$, the constants match the single-scale $k\varepsilon 2$ model contained in the SCIPVIS code. It is not claimed in this paper that these constants should be viewed as universal values without further validation against experiment. Within the context of this paper, the two-scale version of $k\varepsilon 2$ is referred to as $k\varepsilon$2-2S and the two-scale version of $k\varepsilon 2$ with the compressibility correction function ($k\varepsilon$2-cc) is referred to as $k\varepsilon$2-2S-cc.

Table 1

	τ_2	C_{P1}	C_{P21}	C_{T1}	C_{T2}	μ_t
Hanjalic (ref. 5)	$\frac{k_T}{\varepsilon_P}$	2.2	1.8	1.08 $\frac{\varepsilon_P}{\varepsilon_T}$	1.15	$0.09D^*$
Chen (refs. 6, 7)	$\frac{k_P}{\varepsilon_P}$	1.6	1.8	1.15	1.8 $\frac{\varepsilon_T}{\varepsilon_P}$	$0.09D$
Present	$\frac{k_P}{\varepsilon_P}$	1.4	2.0	1.15	1.8 $\frac{\varepsilon_T}{\varepsilon_P}$	$(0.09g - 0.053f)K(M)D$

$^*D = \rho\frac{k_P}{\varepsilon_P}(k_P + k_T)$.

Modified SCIPVIS Model

The $k\varepsilon$2-2S and $k\varepsilon$2-2S-cc turbulence models, described above, were incorporated into the SCIPVIS code to provide a computational framework for testing the importance of two-scale effects. The SCIPVIS code solves the steady-state, parabolized Navier-Stokes equations (streamwise diffusion terms neglected) by a spatial-marching numerical scheme. Utilizing the mapped coordinates, ξ and η, given by the simple rectangular transformation (see ref. 1),

$$\left.\begin{aligned} \xi &= x \\ \eta &= \frac{r - r_L(x)}{r_U(x) - r_L(x)} \end{aligned}\right\} \tag{13}$$

where r_U and r_L are the boundaries of the jet solution domain, equations (1) and (2) can be expressed in the following vector form:

$$\frac{\partial \mathbf{E}}{\partial \xi} + \frac{\partial \mathbf{F}}{\partial \eta} = \frac{b^2}{r^J}\frac{\partial}{\partial \eta}\left(\frac{r^J \mu_{\text{eff}}}{\beta_f}\frac{\partial \mathbf{f}}{\partial \eta}\right) + \mathbf{G}_f \qquad (14)$$

where

$$\mathbf{f} = \begin{bmatrix} 1 \\ U \\ V \\ H \\ \Phi \\ k \\ \varepsilon \\ -- \\ k_T \\ \varepsilon_T \end{bmatrix} \quad \mathbf{E} = \begin{bmatrix} \rho U \\ \alpha P + \rho U^2 \\ \rho UV \\ \rho UH \\ \rho U\Phi \\ \rho Uk \\ \rho U\varepsilon \\ ----- \\ \rho Uk_T \\ \rho U\varepsilon_T \end{bmatrix}$$

$$\mathbf{F} = B\begin{bmatrix} \rho V \\ \rho UV \\ P + \rho V^2 \\ \rho VH \\ \rho V\Phi \\ \rho Vk \\ \rho V\varepsilon \\ ----- \\ \rho Vk_T \\ \rho V\varepsilon_T \end{bmatrix} - A\mathbf{E} = B\mathbf{F}_1 - A\mathbf{E}$$

$$\mathbf{G}_f = \mathbf{G}_1 - A\mathbf{E} - \frac{J}{r}\mathbf{F}_1$$

$$\mathbf{G}_1 = \begin{bmatrix} 0 \\ (\alpha - 1)\frac{\partial P}{\partial x} \\ 0 \\ 0 \\ 0 \\ \underline{P} - \rho\varepsilon \\ (C_{P1}\underline{P} - C_{P2}\rho\varepsilon)\,\varepsilon/k \\ ---------- \\ \rho(\varepsilon_P - \varepsilon_T) \\ \rho\,(C_{T1}\varepsilon_P - C_{T2}\varepsilon_T)\,\frac{\varepsilon}{k} \end{bmatrix}$$

$$A = \frac{(1-\eta)\frac{dr_L}{dx} + \eta\frac{dr_U}{dx}}{r_U - r_L}$$

$$B = \frac{1}{r_U - r_L}$$

For the two-scale models, $k\varepsilon$2-2S and $k\varepsilon$2-2S-cc, k_P should replace k and ε_P should replace ε in the preceding vectors.

In the case of the one-scale model, the **f**, **E**, **F**, $\mathbf{F}_1$, and $\mathbf{G}_f$ arrays contain only the first seven dependent variables, and k_T takes a value of zero. Thus, the only change to the SCIPVIS model needed to incorporate the two-scale turbulence model is the addition of two transport equations to describe the transfer processes.

The solution of these equations is accomplished by using a two-step predictor-corrector explicit algorithm with ξ as the marching direction. Switching between hyperbolic (supersonic, unknown pressure) regions and parabolic (subsonic, known pressure) regions is illustrated by the parameter α. In supersonic regions, $\alpha = 1$; in subsonic regions, $\alpha = 0$. This approach allows elliptic effects (upstream influence) to be taken into account in subsonic regions by specifying the pressure from an auxiliary solution (e.g., solution of the potential equation). However, in this study, the external pressure was assumed to be constant, and elliptic effects were neglected. Further details on the numerical SCIPVIS model are given in reference 1.

Solution of the mapped steady conservation equations requires a knowledge of the initial conditions in order to perform the spatial integration. For the calculations presented in this paper, initial conditions were specified at the start of the jet (corresponding to a nozzle exit) as a "top hat" profile (i.e., uniform jet properties for $r \leq r_j$ and uniform free-stream properties for $r > r_j$. The initialization of turbulence properties is described in the next section.

Results and Discussion

The multiscale (two-scale) model of Hanjalic et al. has been tested in various boundary-layer and free-shear flows (refs. 5, 13, and 17). Chen tested his version of the two-scale model for predicting recirculating flows (ref. 6) and confined swirling-jet flows (ref. 7). The comparisons made in refs. 5, 6, 7, and 17 have perhaps served to show the advantages of including the spectral character of turbulence in traditional second-order closure.

In this section, one-scale and two-scale turbulence closure models are used in the SCIPVIS code to predict the interaction of an imperfectly expanded supersonic jet ($1 < M_j < 2$) with the surrounding external stream. Because of numerical limitations in the SCIPVIS code, calculations could not be made with the external Mach number at exactly zero. Therefore, all calculations presented here are for an external stream at Mach 0.25. Sensitivity studies showed that varying this arbitrary value by as much as ± 0.1 produced no significant effect on the centerline properties.

Throughout this paper, the experimental data are taken from the report of Norum and Seiner (ref. 18).

The following two test cases were selected for study:

1. Underexpanded, cold-air, supersonic jet; $M_j = 2.0, P_j/P_a = 1.45$.
2. Underexpanded, cold-air, sonic jet; $M_j = 1.0, P_j/P_a = 1.62$.

Results for both cases are presented in reference 1 for the one-scale models. Those results include calculations, which are also included here for completeness, made with the kW model of Spalding (ref. 19) for the supersonic jet. The details of the initial profiles and other numerical parameters used for those calculations were not available; therefore, both cases were recalculated for the present study to ensure that comparisons with the two-scale results would be made for the same initial conditions.

In both cases, there is no information available regarding initial turbulence levels. For the present calculations, the initial profiles of k, ε, k_P, k_T, ε_P, ε_T and W are obtained from the mixing-length model based upon the mean-flow profile. The mixing-length model relates μ_t to the local gradient through the relation,

$$\mu_t(r) = \rho \ell^2 \left| \frac{\partial U}{\partial r} \right| \tag{15}$$

where ℓ is an initial mixing-length scale estimated from spread rates for incompressible shear layers (see ref. 20 for details).

Assuming $P/\varepsilon = 1$, then

$$\left.\begin{aligned} k(r) &= \frac{\mu_t(r)\left|\frac{\partial U}{\partial r}\right|}{0.3\rho(r)} \\ \varepsilon(r) &= \frac{0.09\rho(r)k^2(r)}{\mu_t(r)} \end{aligned}\right\} \tag{16}$$

The two turbulent quantities, k and ε, may then be used to estimate the initial profiles for the two-scale quantities, k_P, k_T, ε_P, and ε_T. A nonequilibrium initial state for the turbulence level was assumed. For convenience in describing the initial two-scale distributions, the following relations are defined:

$$\left.\begin{aligned} k_P &= \frac{a}{a+b}(k) \\ k_T &= \frac{b}{a+b}(k) \\ \varepsilon_P &= \varepsilon \\ \varepsilon_T &= \frac{c}{c+d}(\varepsilon_P) \end{aligned}\right\} \tag{17}$$

where b, c, and d are constants with a value of 0.5 and where $a = 1$ in most cases. The absolute values of a, b, c, and d are also used as limiting values of k_P, k_T, ε_P, and ε_T outside the mixing shear layer of the jet. Since the actual values of k_P, k_T, ε_P and ε_T are determined from the discretized initial profiles of U, the magnitudes of initial turbulence and dissipation may depend strongly on the profile shape and number of radial grid points. The effect of these initial values is shown subsequently for the sonic jet.

The spatial integration of equation (14) is provided by SCIPVIS with its several integration options (parabolic, partially parabolic, hyperbolic, and hyperbolic/parabolic).

Underexpanded, Cold-Air, Supersonic Jet; $M_j = 2.0, P_j/P_a = 1.45$

In this section, the calculated results using the $k\varepsilon$2-cc, $k\varepsilon$2-2S-cc, and kW (one-scale) models are compared with the plume experimental data. Identical initial data are used for three different calculated results (i.e., with the same integration options, initial profile, and number of nodes along the radial axis r).

In figure 5, the measured centerline static pressure illustrates the decaying shock structure that occurs as a result of the interaction of the shocks with the growing mixing layer. The jet is operated at a pressure ratio of 1.45, which corresponds to a fully expanded Mach number of 2.24, and is issued from a convergent-divergent nozzle with a design Mach number of 2. Figure 6 shows a comparison of the results predicted using the different turbulence models with the measured streamwise pressure variation along the jet centerline. This figure shows that the $k\varepsilon$2-cc turbulence model (fig. 6(a)), incorporated with the SCIPVIS code, predicts the pressure variations up to the first five shock cells and significantly underestimates the rest of the shock-cell decay. The same observations have been made by Dash and Wolf (ref. 21) for this $k\varepsilon$2-cc model, which indicates that the growth of the mixing region and turbulent dissipation are not properly modeled using the $k\varepsilon$2-cc one-scale model.

Figure 6(b) shows the calculated results using the $k\varepsilon$2-2S-cc model compared with the measured data. This comparison shows that, using the $k\varepsilon$2-2S-cc turbulence model, the prediction of centerline pressure variations is much improved over $k\varepsilon$2-cc model predictions. The shock-cell spacings and pressure amplitudes agree extremely well up to 40 jet radii.

Finally, figure 6(c) shows the calculated results and comparisons with experiment using the kW turbulence model. The kW model also shows excellent agreement with experiment as was also observed in reference 1. The agreement with experiment for both a one-scale (kW) model and a two-scale ($k\varepsilon$2-2S-cc) model indicates that multiscale effects are probably not very important in this Mach 2 case. In fact, all three models predict the overall axial decay in

peak shock-cell pressures reasonably well, although there is considerable disagreement in phase in the axial direction for the $k\varepsilon$2-cc results.

Comparisons of turbulence intensity between $k\varepsilon$2-cc and kW model predictions and experiment have been presented in reference 3 and reasonably good agreement has been obtained. The present two-scale model gives similar agreement. However, because of the limited amount of data available, no conclusion can be drawn as to which model provides better prediction of turbulence intensity. For the Mach 2 jet, it is concluded that the centerline pressure predictions are not extremely sensitive to the details of turbulence in the near-field mixing region.

Underexpanded, Cold-Air Sonic Jet;
$M_j = 1.0, P_j/P_a = 1.62$

The experimental results shown in figure 7 are for the underexpanded condition ($P_j/P_a = 1.62$) for a sonic nozzle (ref. 3). This pressure ratio corresponds to a fully expanded Mach number of 1.37, and this figure shows that the measured data appear to decay abruptly after the fifth shock cell ($x/r_j > 10$). Although there are no flow-field data available to explain this uncharacteristic rapid decay, acoustic data obtained under similar jet conditions suggest that such phenomena may be caused by acoustic resonance. Further supporting measurements have shown that for jets exhibiting strong resonance behavior, the jet-plume shock structure decays rapidly beyond the jet potential core. In such cases, it is postulated that acoustic waves generated by the shock-cell structure feed upstream through the subsonic portion of the mixing layer at a frequency that causes the rapid growth of turbulent instabilities which eventually dominate the plume structure.

Basic model comparisons. As with most marching codes, SCIPVIS was not able to run with the exit Mach number set precisely at 1.0. A Mach number of 1.02 is used as an initial value for the calculations discussed in this section. Figure 8 shows the results predicted with the $k\varepsilon$2-cc, $k\varepsilon$2-2S-cc, and kW turbulence models compared with measured centerline pressures. All three calculations show reasonably good agreement up through the first five shock cells, although there is some disagreement in amplitude after the first cell. However, all three calculations greatly underpredict the shock-cell decay after the fifth cell. Comparing the various calculated results, the $k\varepsilon$2-2S-cc and kW turbulence models show a faster shock-cell decay than the $k\varepsilon$2-cc predictions, and the two-scale results show the most rapid decay of any of the models. It has not been determined that these disagreements with experiment are related only to turbulence modeling; they may also be caused by the limitations of the basic computational model. That is, if acoustic resonance is occurring through upstream influence in the subsonic portion of the mixing layer, elliptic effects (which are absent in the present calculations) must be considered. It is clear from these comparisons that none of the three turbulence models ($k\varepsilon$2-2S-cc, $k\varepsilon$2-cc, or kW) provide an accurate representation of the flow field of the sonic jet.

The experimental results for underexpanded jet flows show that after the jet initial mixing region, the average static pressure falls below atmospheric. Near the end of the transition zone, there is a general recovery of the centerline static pressure (ref. 3). This phenomenon shows that the pressure in the subsonic region of the shear layer varies with x/r_j. The SCIPVIS code is constructed to solve the parabolized Navier-Stokes (PNS) equations and assumes that the pressure P in the elliptic (subsonic) zone is constant and equal to the upper boundary pressure of this region (atmospheric). Thus, the calculated static-pressure distribution shown in figure 8 always falls symmetrically on the atmospheric line.

Effect of compressibility. Based on the assumption that incompressible turbulence models may be used to solve mixing-layer compressible flows for turbulent Mach numbers close to and less than 1, it is worthwhile to drop the compressibility correction function and repeat the calculation using the $k\varepsilon$2 and $k\varepsilon$2-2S turbulence models. Figure 9(a) shows the effect of dropping the compressibility correction on the results of the $k\varepsilon$2 turbulence model for the sonic jet and figure 9(b) shows the $k\varepsilon$2 results compared with experiment. Even without the compressibility correction function, the $k\varepsilon$2 underestimates the turbulent mixing of the jet. Again, this indicates that the growth of the mixing region and turbulent dissipation are not properly modeled using the $k\varepsilon$2 model.

Figure 10(a) shows the effect of dropping the compressibility correction on the calculated results using the two-scale ($k\varepsilon$2-2S) turbulence model. Figure 10(b) shows the superposition of the calculated and measured pressure distributions. As can be seen, dropping the compressibility correction has a significant effect on the two-scale model predictions. The $k\varepsilon$2-2S result shows a rapid decay in centerline pressure beyond the jet potential core and shows a very favorable improvement in the agreement with experiment compared with the $k\varepsilon$2 result (compare figs. 9(b) and 10(b)). Even though the axial locations of all shock cells do not match the experiment, it is clear that the two-scale turbulence model, $k\varepsilon$2-2S, provides a better representation of the overall

shock-cell decay (and therefore the turbulent mixing) than either of the one-scale models ($k\varepsilon 2$ or kW).

Figure 11 shows a comparison between the total turbulent kinetic energies calculated using the $k\varepsilon 2$ (dashed line) and the $k\varepsilon$2-2S (solid line) turbulence models. The $k\varepsilon$2-2S calculation shows a rapid increase in total turbulent kinetic energy beyond $x/r_j = 15$ which corresponds closely to the observed rapid decay in centerline static pressure. On the other hand, the $k\varepsilon 2$ turbulence model calculation shows a slow increase in centerline total kinetic energy.

Effect of initial conditions. At this point it is worthwhile to study the effect of the initial and limiting values of kinetic energy and dissipation (transfer region) on the calculated results of the $k\varepsilon$2-2S turbulence model. Results for the following two additional cases are presented:

1. Case 1—$d = 0.125$ ft^2/sec^3 (reduced ε_T)
2. Case 2—$b = 2$ ft^2/sec^2 (increased k_T)

These cases correspond to a constant time-scale ratio T of 8, whereas a ratio of 2 was used for the previous calculations. The initial values of k_P and ε_P assume the same values used in the previous calculations (i.e., $a = 0.5$ ft^2/sec^2 and $c = 1$ ft^2/sec^3). The values of a, b, and c are used to calculate the initial profiles of k_P, k_T, ε_P, and ε_T as described previously.

Figure 12 shows comparisons between the centerline pressure distributions calculated for these two cases and the results shown previously for $k\varepsilon$2-2S (fig. 10). In general, both cases with the higher time-scale ratio show a slight increase in the shock-cell decay over the original calculations. Case 2 (fig. 12(b)) shows a slightly faster decay in the centerline pressure than case 1 (fig. 12(a)) but appears to affect the amplitude of pressure (shock strength) in the near field of the jet (immediately after the first shock cell) earlier than it should.

Figure 13 shows the variation of the time-scale ratio along the jet centerline for cases 1 and 2 compared with the original result. All three calculations produce approximately the same value of T in the far field ($x/r_j > 10$). For case 2, however, the value of T starts increasing earlier ($x/r_j > 2.5$) than for the other cases. This would appear to be related to the earlier turbulence mixing and decaying of the shock strength produced by this case. Based on these and similar calculations for other values of T, it may be speculated that the turbulence mixing of the plume is somehow related to the time ratio T.

Modified time-scale model. It is suggested in references 5 to 7 that some of the "constants" in the turbulent transport equations for k_P, ε_P, k_T, and ε_T may somehow vary with the production and transfer mechanisms. Based on the experimental data for the Mach 1 jet, it is obvious that some mechanism is needed to explain the rapid decay in centerline pressure for $x/r_j > 10$. To test the capability of the two-scale formulation to "model" such a mechanism, it would appear that one option is to relate one or more of the constants in the turbulent-transport equations to the time ratio T. From the results shown in figure 13, it is seen that the predicted time ratio T drops to values less than one for $x/r_j > 10$. Therefore, the two-scale model was modified by replacing the term $\rho\varepsilon_T$ with $F(T)\rho\varepsilon_T$ in the k_T transport equation. The following arbitrary functions for $F(T)$ are proposed in this study:

$k\varepsilon$2-2S-T1

$$F(T) = \begin{cases} 1 & (T > 1) \\ T & (T \leq 1) \end{cases} \tag{18}$$

and

$k\varepsilon$2-2S-T2

$$F(T) = \begin{cases} 1/T & (T > 1) \\ T & (T \leq 1) \end{cases} \tag{19}$$

Each of these functions is constructed so as to decrease the effective transfer dissipation for $T < 1$ and to thereby increase the transfer kinetic energy and, presumably, the turbulent mixing in the downstream region of the jet.

Figure 14 shows a comparison between the centerline pressure predictions using the $k\varepsilon$2-2S-T1 model and the $k\varepsilon$2-2S model and between the $k\varepsilon$2-2S-T1 model and experiment. In general, the $k\varepsilon$2-2S-T1 model shows a slight improvement in the calculated results over the $k\varepsilon$2-2S model. In the near field, both models have the same pressure variations; in the far field, there is a slight decrease in shock-cell spacing. Figure 15 shows a similar comparison of the $k\varepsilon$2-2S-T2 results with $k\varepsilon$2-2S and experiment. The $k\varepsilon$2-2S-T2 model shows a very rapid decay in the centerline static pressure compared with $k\varepsilon$2-2S and shows a faster decay than even the experimental results. Figure 16 shows the comparison between total kinetic energy produced by $k\varepsilon$2-2S, $k\varepsilon$2-2S-T1, and $k\varepsilon$2-2S-T2 turbulence models. The $k\varepsilon$2-2S-T2 calculation shows a rapid increase in turbulence total kinetic energy near $x/r_j = 10$, which corresponds closely to the observed rapid decay of centerline static pressure. On the other hand, the calculation of the $k\varepsilon$2-2S turbulence model shows a slower increase in centerline total kinetic energy, which starts at about an $x/r_j = 15$. (The rise in centerline turbulent kinetic energy occurs as the mixing reaches the axis of the jet.)

The $k\varepsilon$2-2S-T1 and $k\varepsilon$2-2S-T2 model results appear to approximately bound the experimental centerline pressure distribution, at least insofar as the overall pressure decay is concerned. However, none of the model predictions gives good results for both shock-cell decay and spacing. Since a major deficiency of the present computational model is the neglect of upstream influence of pressure disturbances on the turbulent mixing and shock interaction, it would be interesting to study these effects using a computational model that could fully account for these elliptic effects. For proper modeling of jet plumes where such strong resonance behavior occurs, such a computational model appears to be essential.

Concluding Remarks

In the present paper, a modified version of the multiscale turbulence model of Hanjalic is applied to the problem of supersonic jets exhausting into still air. In particular, the problem of shock-cell decay through turbulent interaction with the mixing layer has been addressed for both mildly interacting and strongly resonant jet conditions. This two-scale model takes into account the nonequilibrium spectral-energy transfer mechanism. The key to the two-scale model is the recognition that, while the one-scale dissipation and kinetic-energy equations contain both production and dissipation terms, these processes occur in different spectral regions. The turbulent-energy production occurs in the large eddies in the flow while dissipation phenomena involve primarily the smaller scales. Steady-state, parabolized versions of the Hanjalic model with ($k\varepsilon$2-2S-cc) and without ($k\varepsilon$2-2S) compressibility corrections were incorporated into the SCIPVIS code to provide a computational framework for testing the validity of the two-scale model.

In general, this investigation has shown that the two-scale model provides significant improvement in the prediction of the plume structure for underexpanded supersonic (Mach 2) and sonic (Mach 1) jets. For the supersonic jet case studied, excellent agreement was obtained with experimental data for the shock-cell pressure decay along the jet centerline up to 40 jet radii. For the sonic jet case, the agreement with experiment was not as good, but the two-scale model still showed significant improvement over one-scale turbulence model results. Although exact agreement was not obtained in the sonic jet, it has been shown that by relating certain coefficients in the turbulent transport equations to the relative time scale for transfer of energy between turbulent scales, the two-scale model can provide predictions that approximately bound the experimental data.

It has been suggested that the present turbulence model be incorporated into a computational model that can account for elliptic effects (e.g., global-relaxation parabolized Navier-Stokes or time-dependent Navier-Stokes methods). That is, in order to simulate the acoustic resonance occurring through upstream influence in the subsonic portion of the mixing layer, elliptic effects (which are absent in the present calculations) must be considered.

NASA Langley Research Center
Hampton, Virginia 23665-5225
April 14, 1987

References

1. Dash, Sanford M.; and Wolf, David E.: *Fully-Coupled Analysis of Jet Mixing Problems, Part I: Shock-Capturing Model, SCIPVIS.* NASA CR-3761, 1984.
2. Tam, Christopher K. W.; Jackson, Jay A.; and Seiner, J. M.: A Multiple-Scales Model of the Shock-Cell Structure of Imperfectly Expanded Supersonic Jets. *J. Fluid Mech.*, vol. 153, Apr. 1985, pp. 123–149.
3. Seiner, John M.; Dash, Sanford M.; and Wolf, David E.: Shock Noise Features Using the SCIPVIS Code. AIAA-83-0705, Apr. 1983.
4. Seiner, John M.: Advances in High Speed Jet Aeroacoustics. AIAA-84-2275, Oct. 1984.
5. Hanjalic, K.; Launder, B. E.; and Schiestel, R.: Multiple-Time-Scale Concepts in Turbulent Transport Modelling. *Turbulent Shear Flows 2,* L. J. S. Bradbury, F. Durst, B. E. Launder, F. W. Schmidt, and J. H. Whitelaw, eds., Springer-Verlag Berlin Heidelberg New York, 1980, pp. 36–49.
6. Chen, C. P.: *Multiple-Scale Turbulence Closure Modeling of Confined Recirculating Flows.* NASA CR-178536, 1985.
7. Chen, C. P.: *Confined Swirling Jet Predictions Using a Multiple-Scale Turbulence Model.* NASA CR-178484, 1985.
8. Hanjalic, K.; and Launder, B. E.: A Reynolds Stress Model of Turbulence and Its Application to Thin Shear Flows. *J. Fluid Mech.*, vol. 52, pt. 4, Apr. 25, 1972, pp. 609–638.
9. Launder, B. E.; Reece, G. J.; and Rodi, W.: Progress in the Development of a Reynolds-Stress Turbulence Closure. *J. Fluid Mech.*, vol. 68, pt. 3, Apr. 15, 1975, pp. 537–566.
10. Wilcox, David C.: Multiscale Model for Turbulent Flows. AIAA-86-0029, Jan. 1986.
11. Tennekes, H.; and Lumley, J. L.: *A First Course in Turbulence.* M.I.T. Press, c.1972.
12. Morkovin, Mark V.: Effects of Compressibility on Turbulent Flows. *The Mechanics of Turbulence,* Gordon & Breach Sci. Publ., Inc., c.1964, pp. 367–380.
13. Fabris, G.; Harsha, P. T.; and Edelman, R. B.: *Multiple-Scale Turbulence Modeling of Boundary Layer Flows for Scramjet Applications.* NASA CR-3433, 1981.
14. Rodi, Wolfgang: *Turbulence Models and Their Application in Hydraulics,* Second rev. ed. International Association for Hydraulic Research, 1984.
15. Launder, B. E.; Morse, A.; Rodi, W.; and Spalding, D. B.: Prediction of Free Shear Flows—A Comparison of the Performance of Six Turbulence Models. *Free Turbulent Shear Flows. Volume I—Conference Proceedings,* NASA SP-321, 1973, pp. 361–426.
16. Dash, S.; Weilerstein, G.; and Vaglio-Laurin, R.: *Compressibility Effects in Free Turbulent Shear Flows.* AFOSR-TR-75-1436, U.S. Air Force, Aug. 1975. (Available from DTIC as AD A016 535.)
17. Cousteix, J.; Houdeville, R.; Arnal, D.; Cler, A.; Berrue, P.; Dubois, P.; and Tulapurkara, E. G.: Comparison of Computation With Experiment. *Complex Turbulent Flows—The 1980–81 AFOSR-HTTM-Stanford Conference on Complex Turbulent Flows: Comparison of Computation and Experiment, Volume III—Comparison of Computation With Experiment, and Computors' Summary Reports,* S. J. Kline, B. J. Cantwell, and G. M. Lilley, eds., Stanford Univ., 1982, pp. 1326–1336.
18. Norum, Thomas D.; and Seiner, John M.: *Measurements of Mean Static Pressure and Far-Field Acoustics of Shock-Containing Supersonic Jets.* NASA TM-84521, 1982.
19. Spalding, D. B.: Concentration Fluctuations in a Round Turbulent Free Jet. *Chem. Eng. Sci.*, vol. 26, no. 1, Jan. 1971, pp. 95–107.
20. Dash, Sanford M.; Pergament, Harold S.; and Thorpe, Roger D.: *Computational Models for the Viscous/Inviscid Analysis of Jet Aircraft Exhaust Plumes.* NASA CR-3289, 1980.
21. Dash, S. M.; and Wolf, D. E.: Interactive Phenomena in Supersonic Jet Mixing Problems. AIAA-83-0288, Jan. 1983.

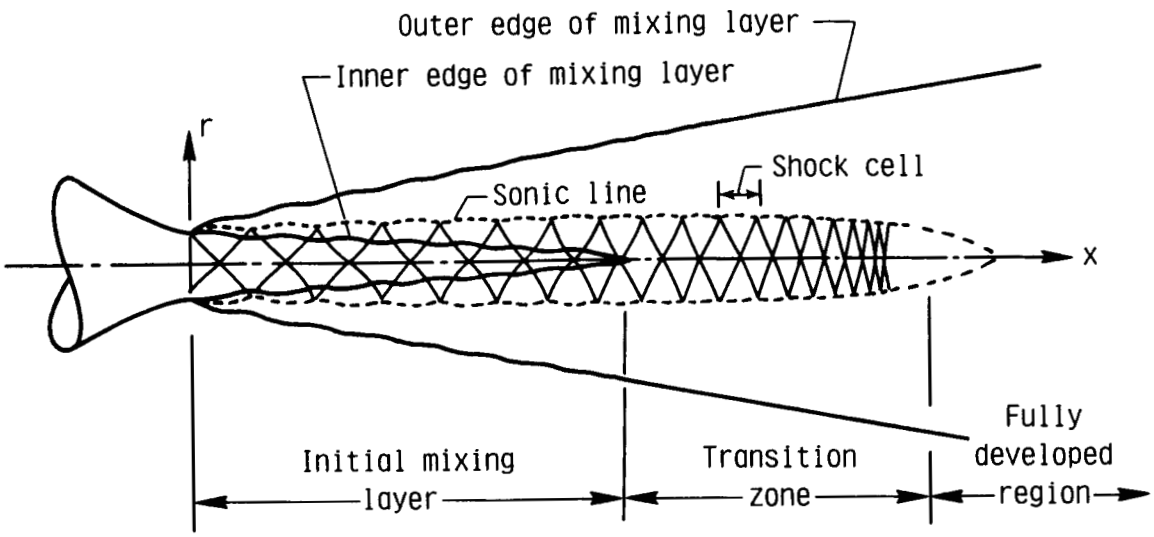

Figure 1. Typical flow field for underexpanded supersonic jet.

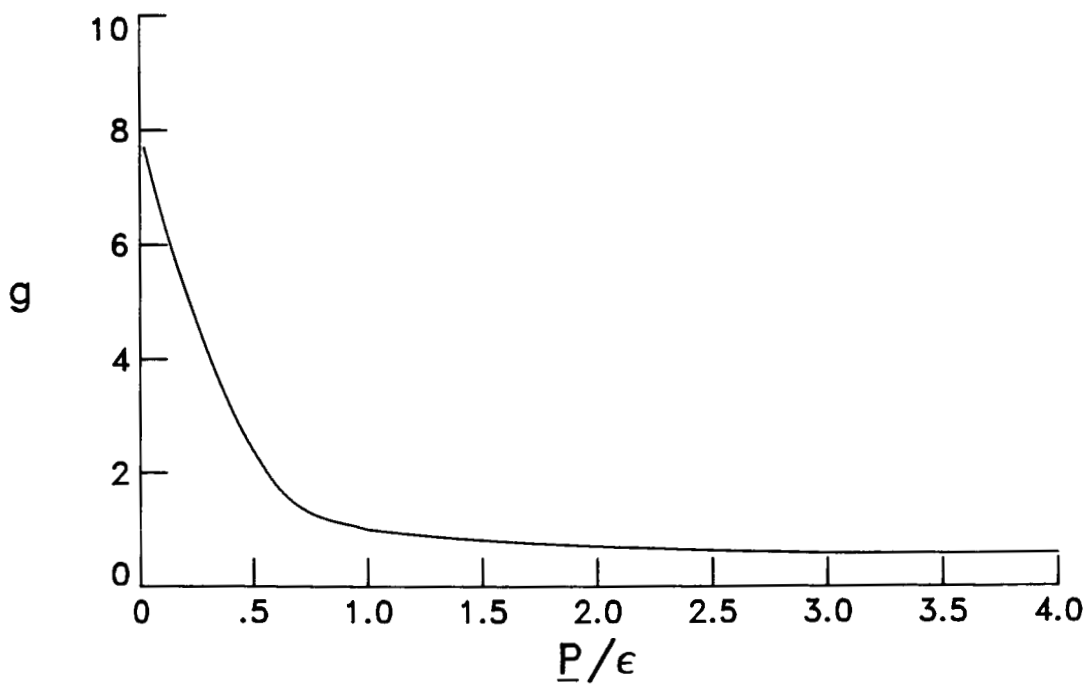

Figure 2. Variation of g with $\underline{P}/\varepsilon$ for $k\varepsilon 2$ turbulence model. (From ref. 1.)

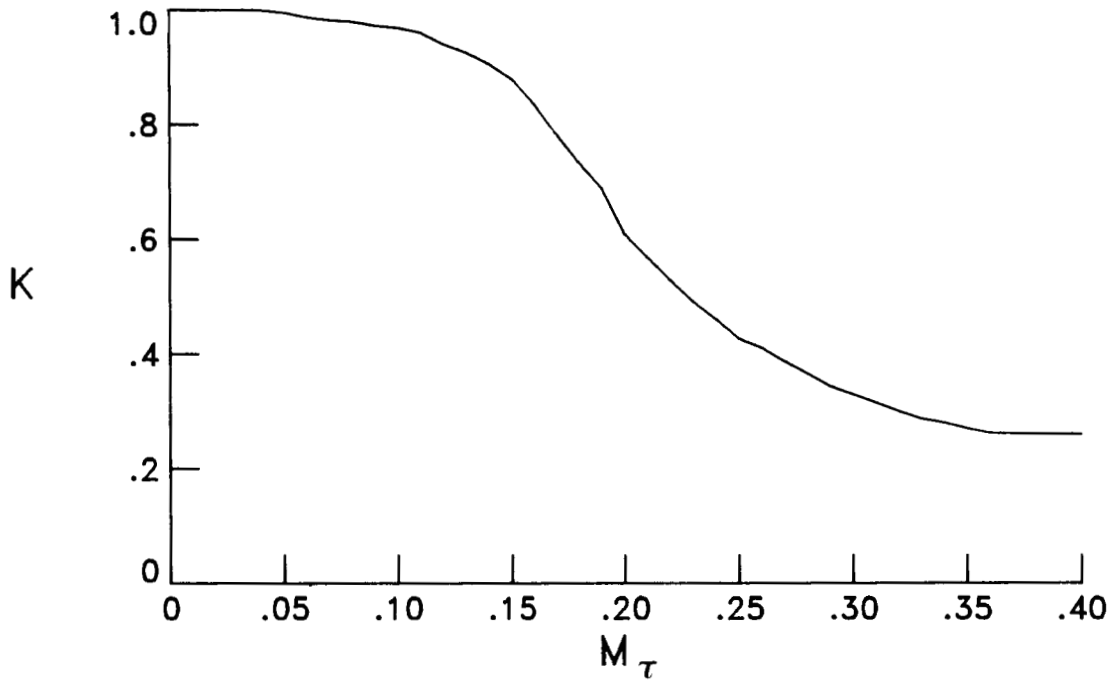

Figure 3. Compressibility correction factor for $k\varepsilon 2$ turbulence model. (From ref. 1.)

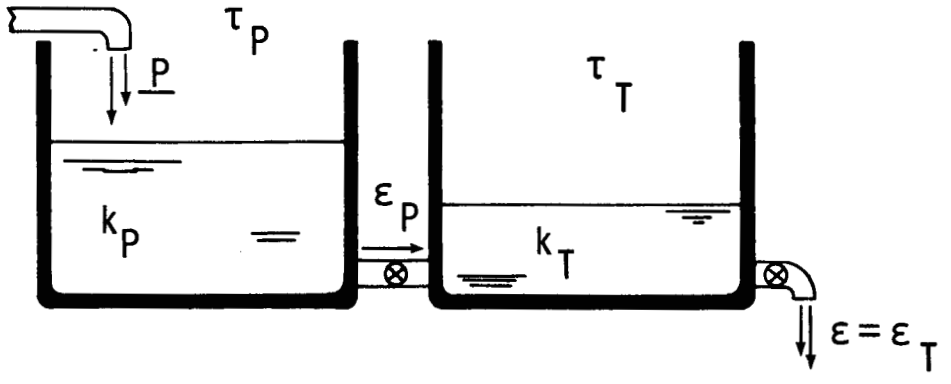

Figure 4. Tank-and-tube analogy for spectral transfer of turbulent energy. (From ref. 5.)

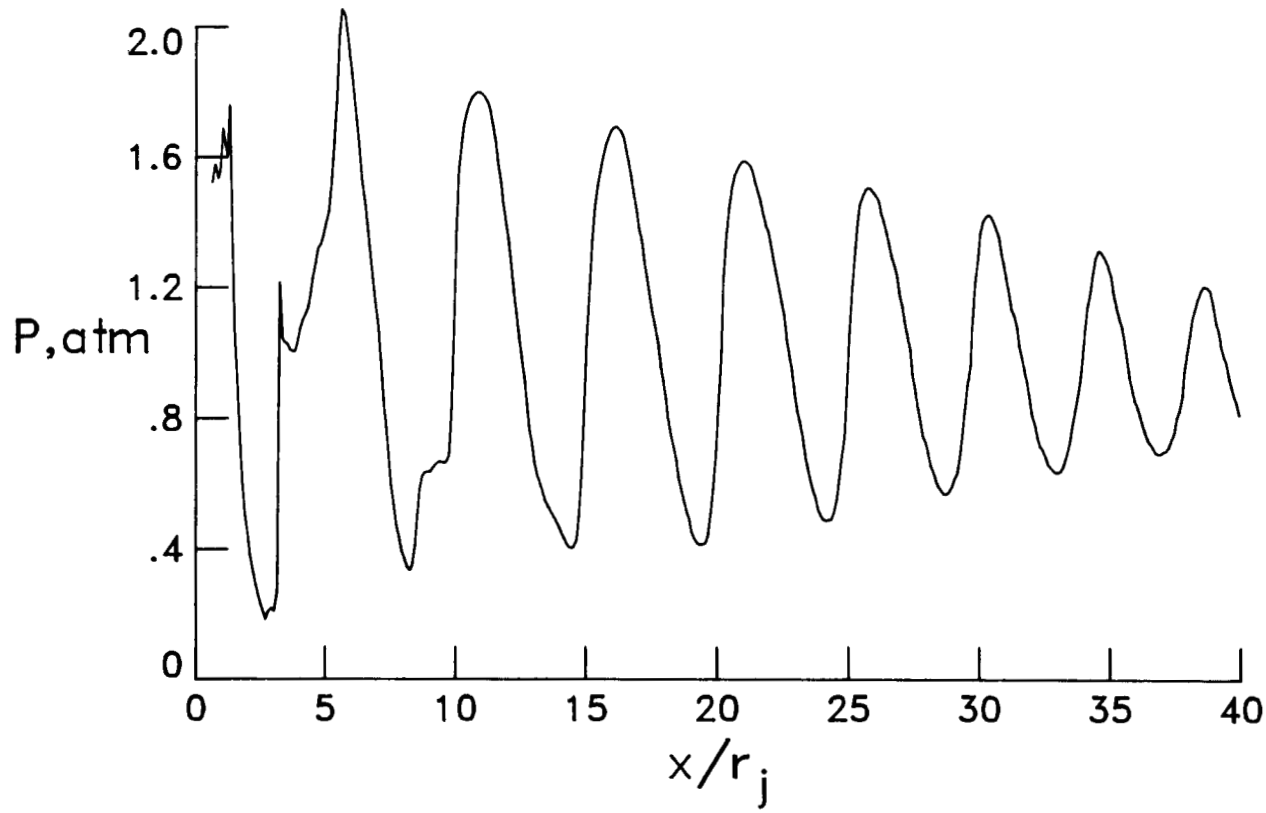

Figure 5. Measured plume centerline pressure distribution for supersonic jet. $M_e = 2.24$; $M_j = 2.0$; $P_j/P_a = 1.45$. (Data from ref. 18.)

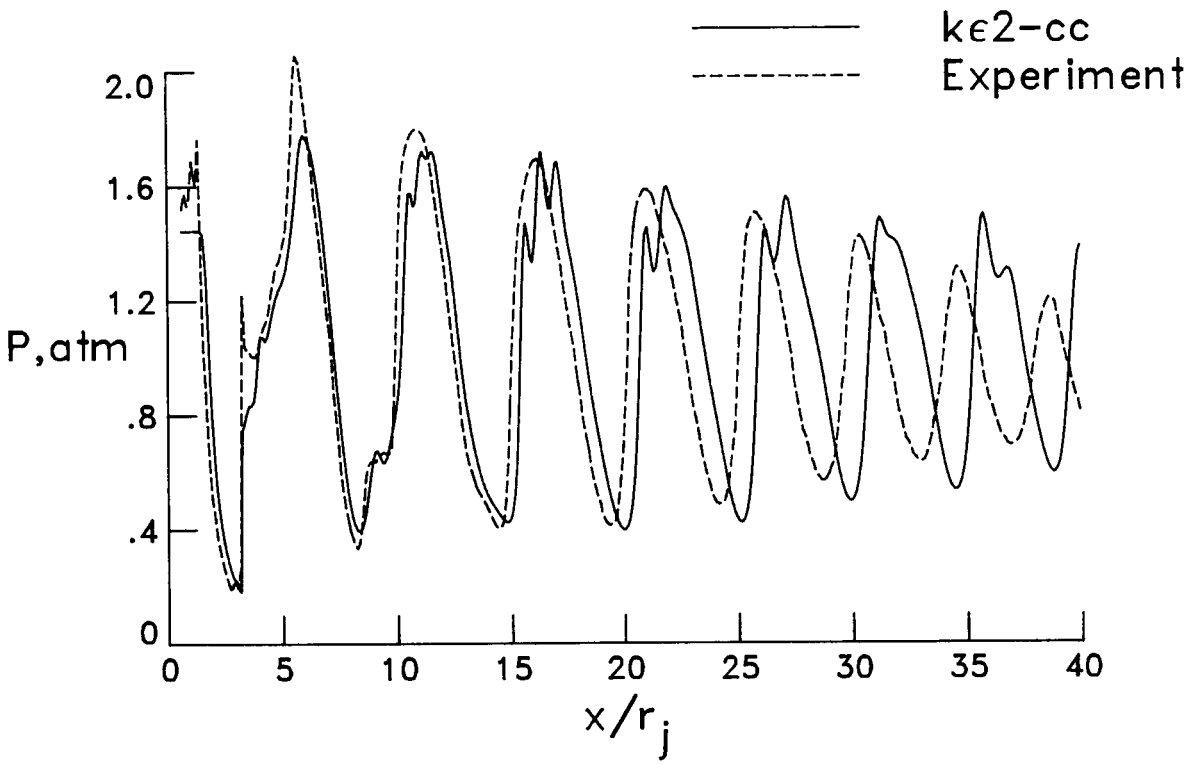

(a) $k\varepsilon$2-cc turbulence model.

Figure 6. Comparison of predicted and measured centerline pressure for supersonic jet.

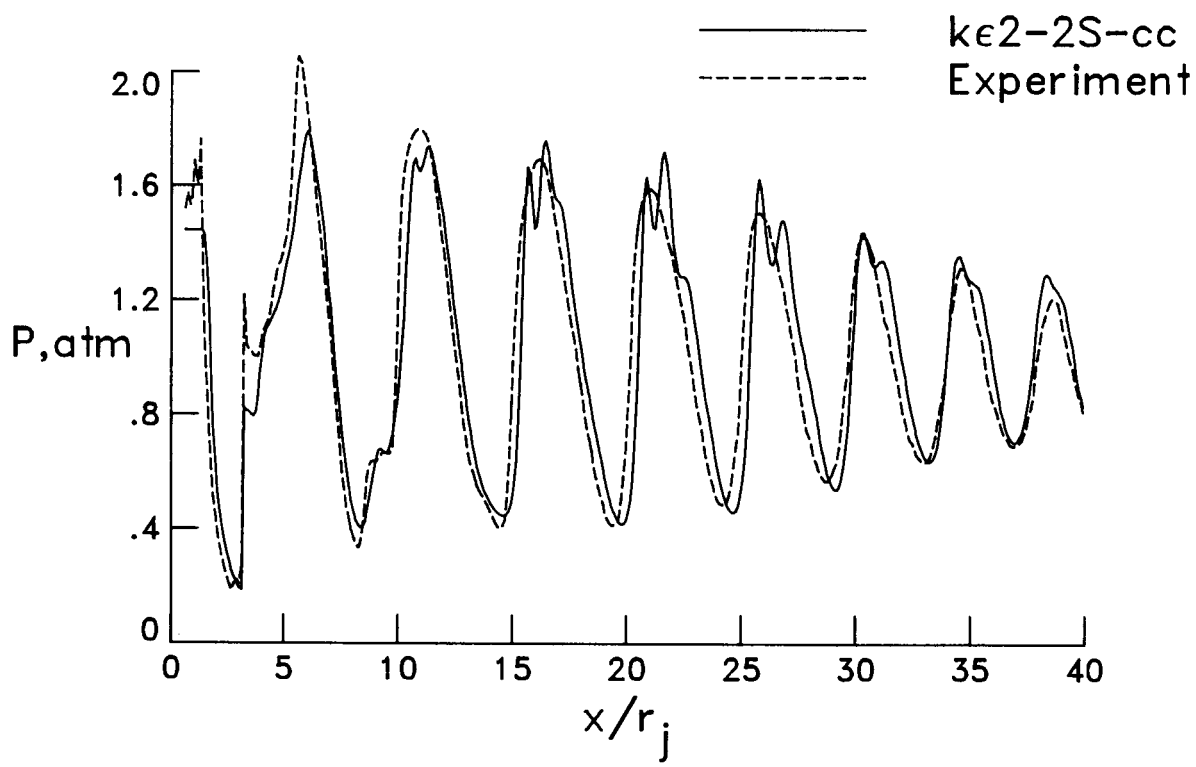

(b) $k\varepsilon$2-2S-cc turbulence model.

Figure 6. Continued.

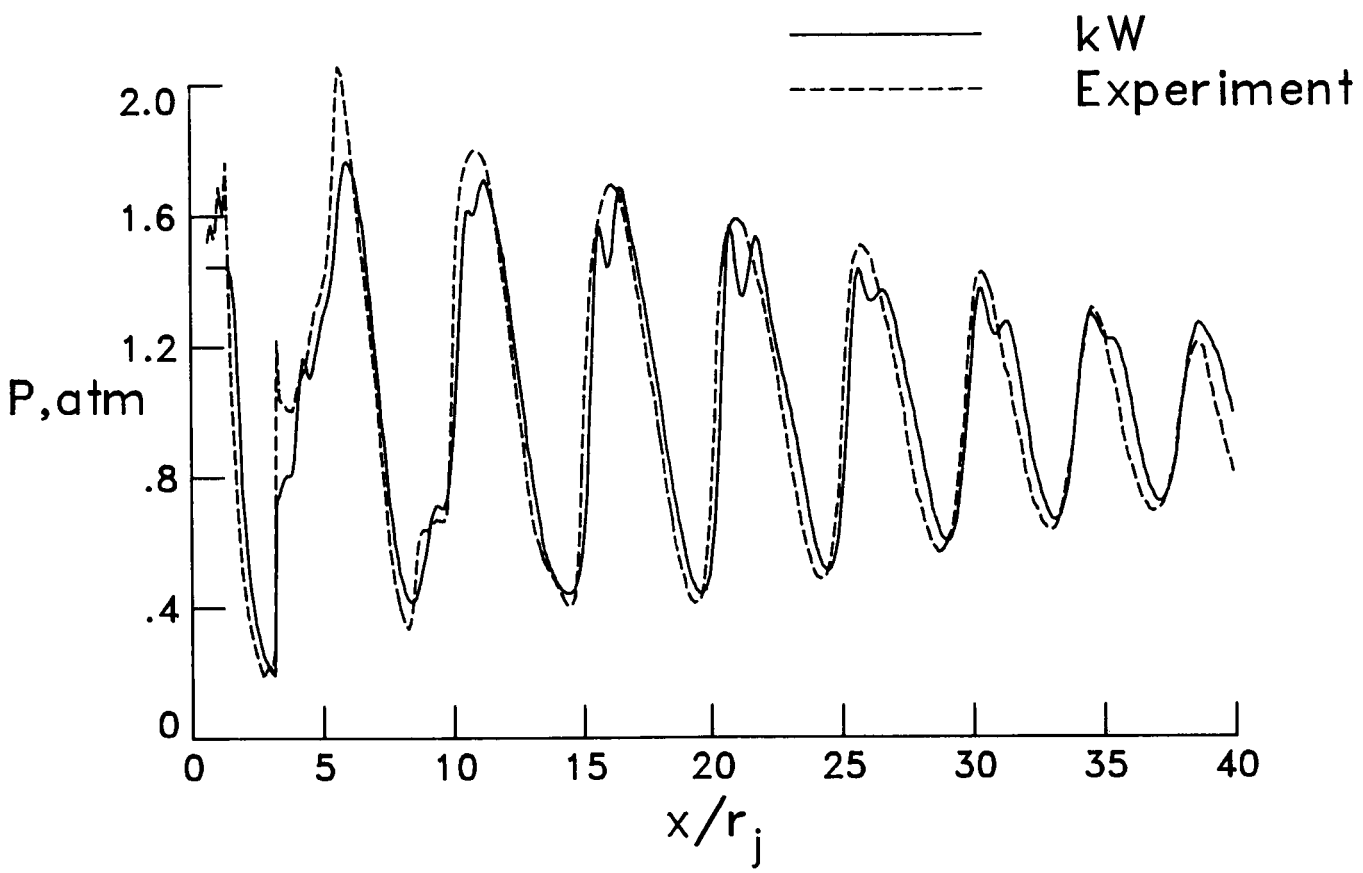

(c) *kW* turbulence model.

Figure 6. Concluded.

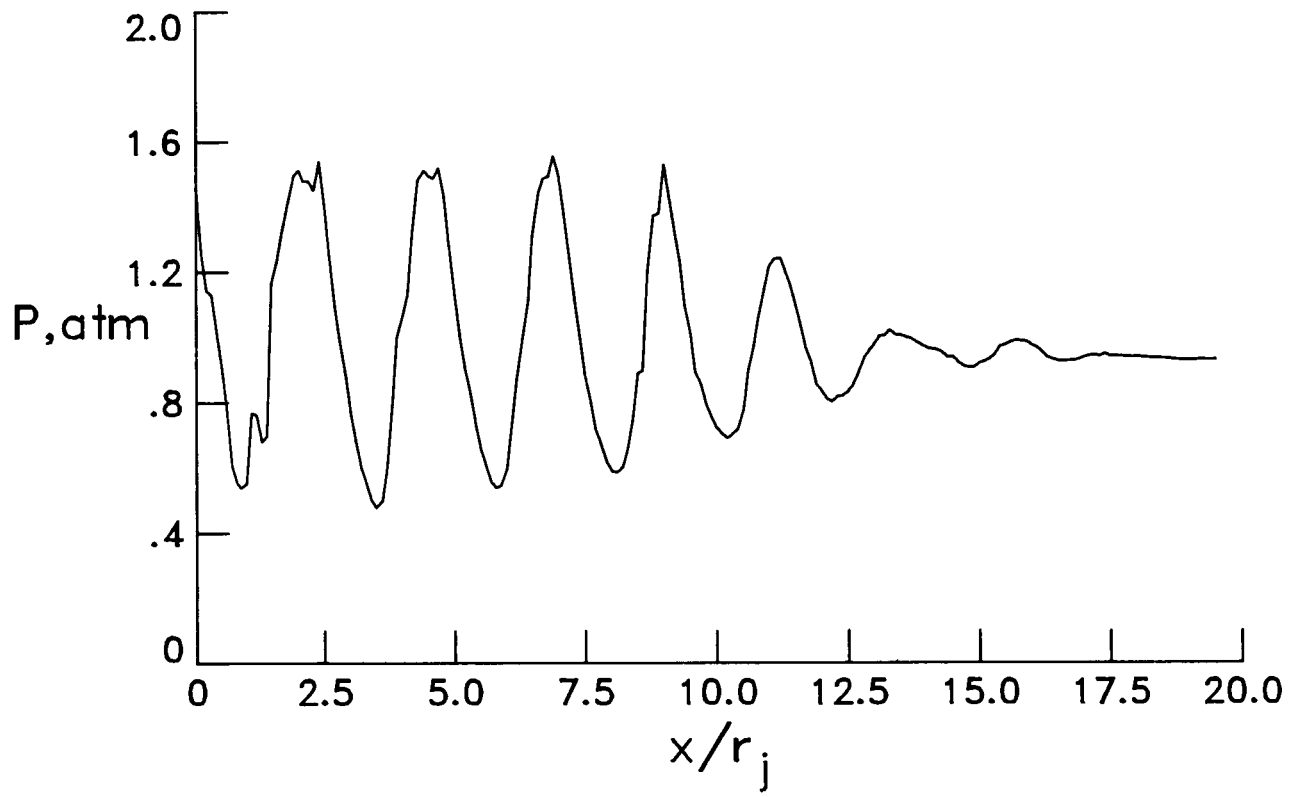

Figure 7. Measured plume centerline pressure distribution for sonic jet. $M_e = 1.37$; $M_j = 1.0$; $P_j/P_a = 1.62$. (Data from ref. 18.)

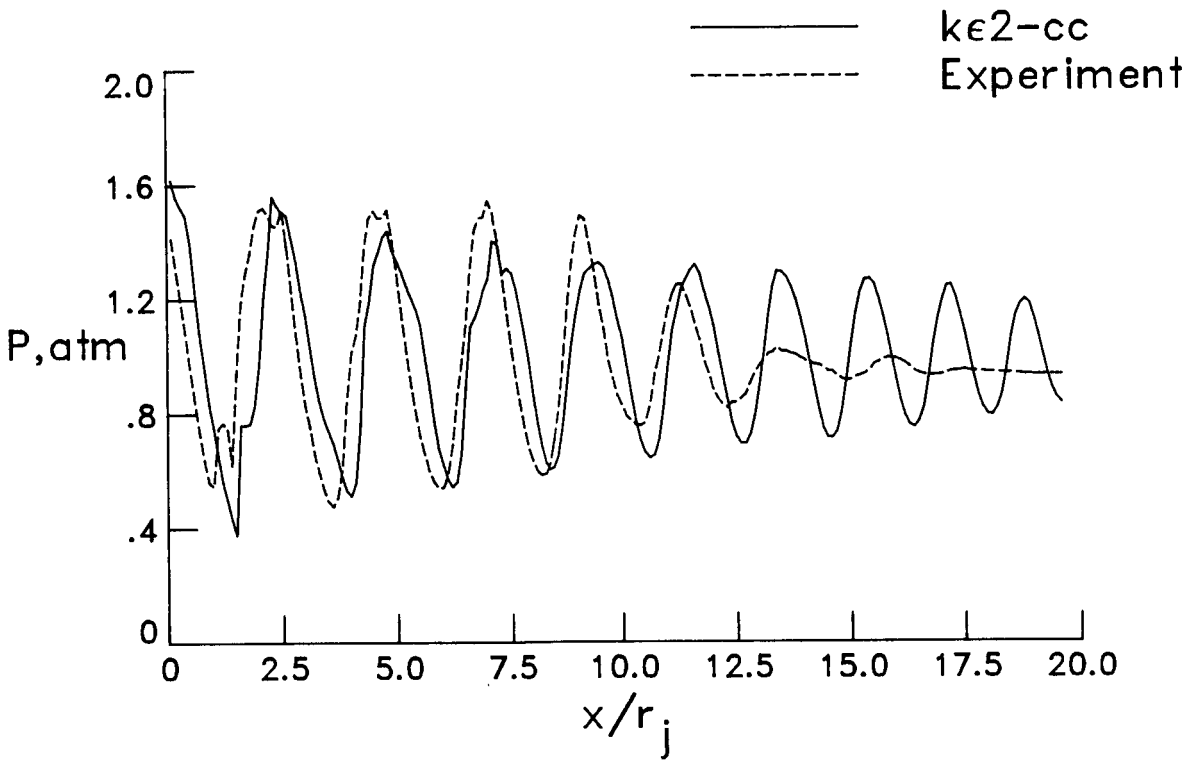

(a) $k\varepsilon$2-cc turbulence model.

Figure 8. Comparison of predicted and measured centerline pressures for sonic jet.

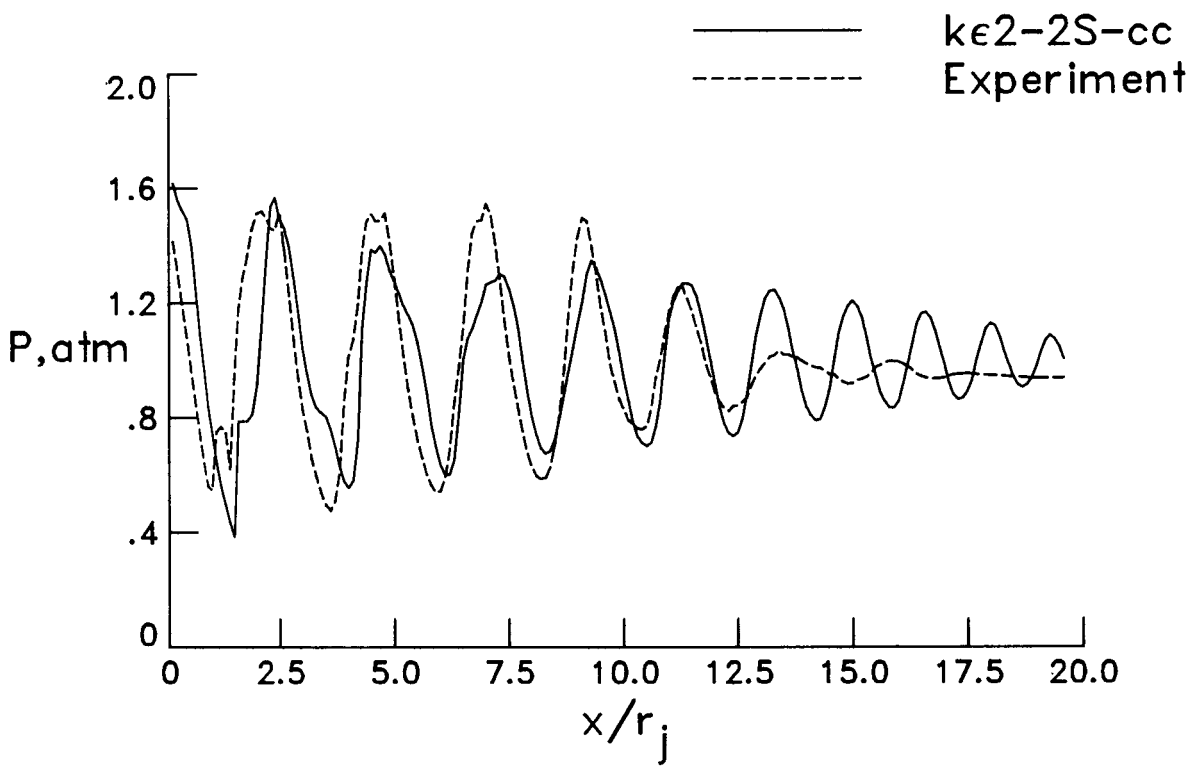

(b) $k\varepsilon$2-2S-cc turbulence model.

Figure 8. Continued.

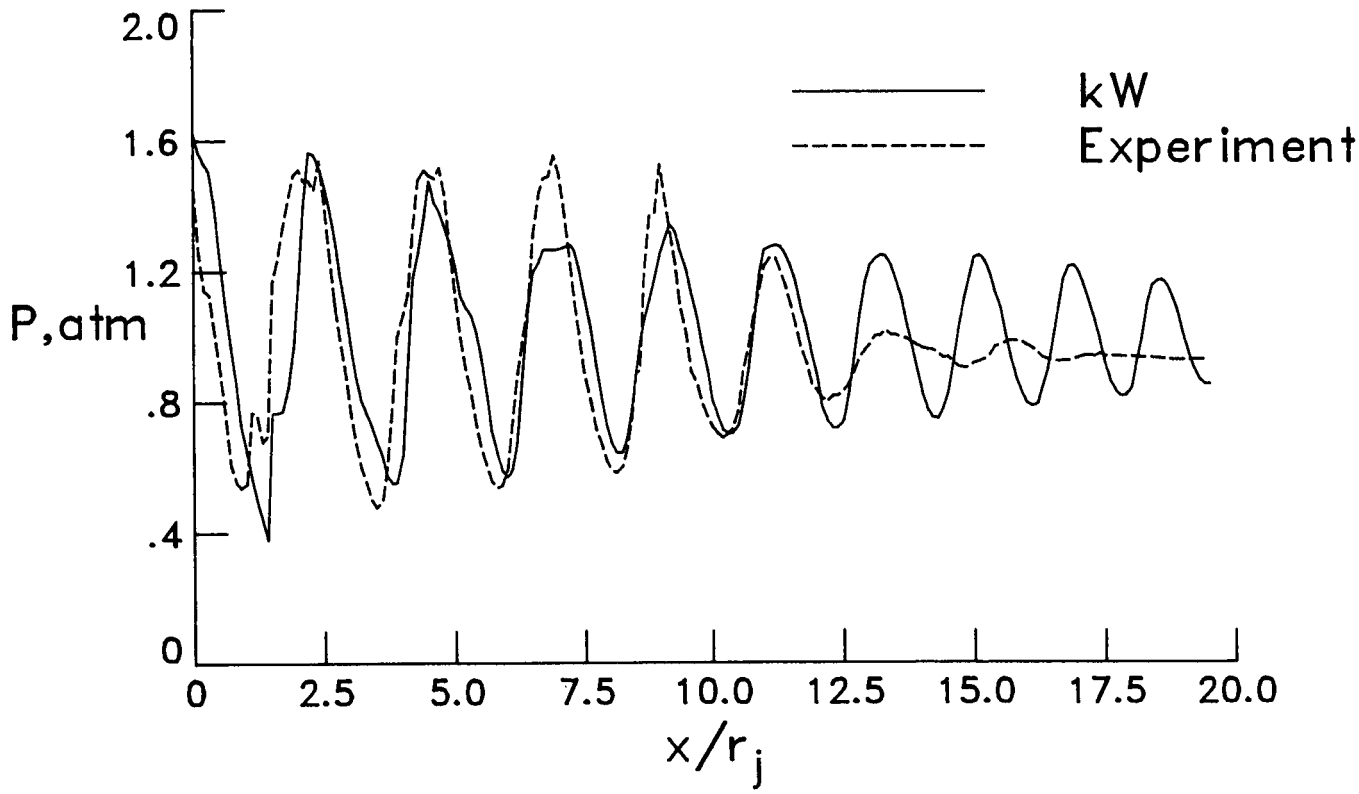

(c) *kW* turbulence model.

Figure 8. Concluded.

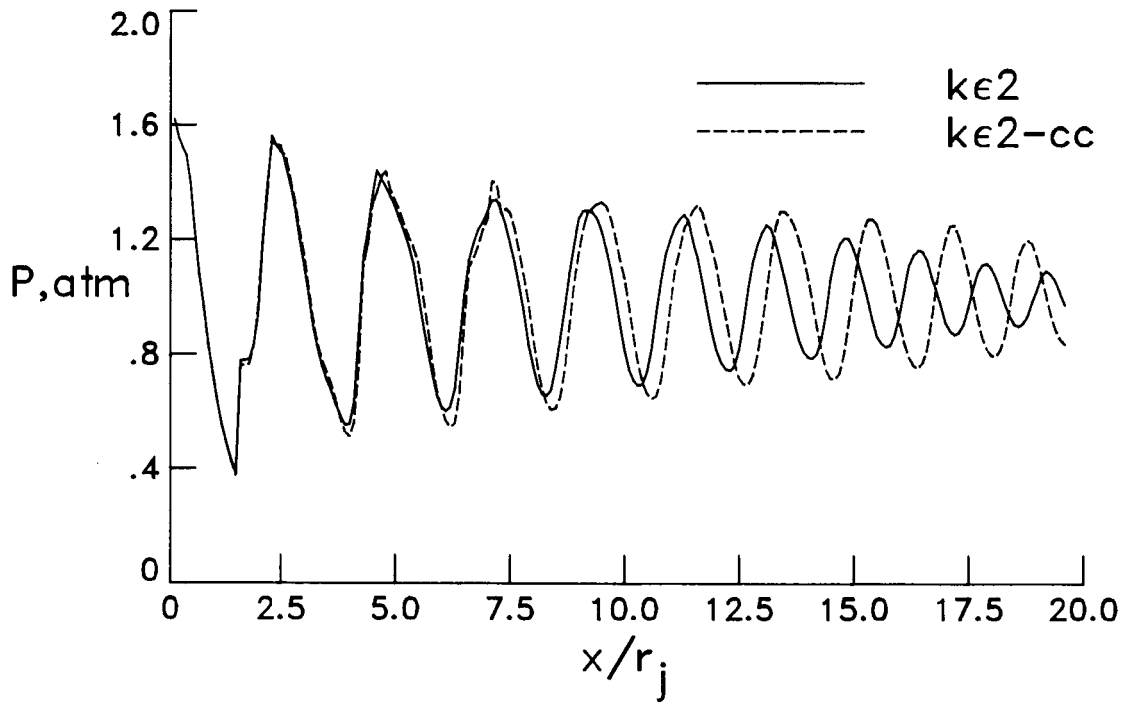

(a) Comparison between $k\varepsilon 2$ and $k\varepsilon 2$-cc.

Figure 9. Effect of compressibility correction on one-scale $k\varepsilon 2$ predictions for sonic jet.

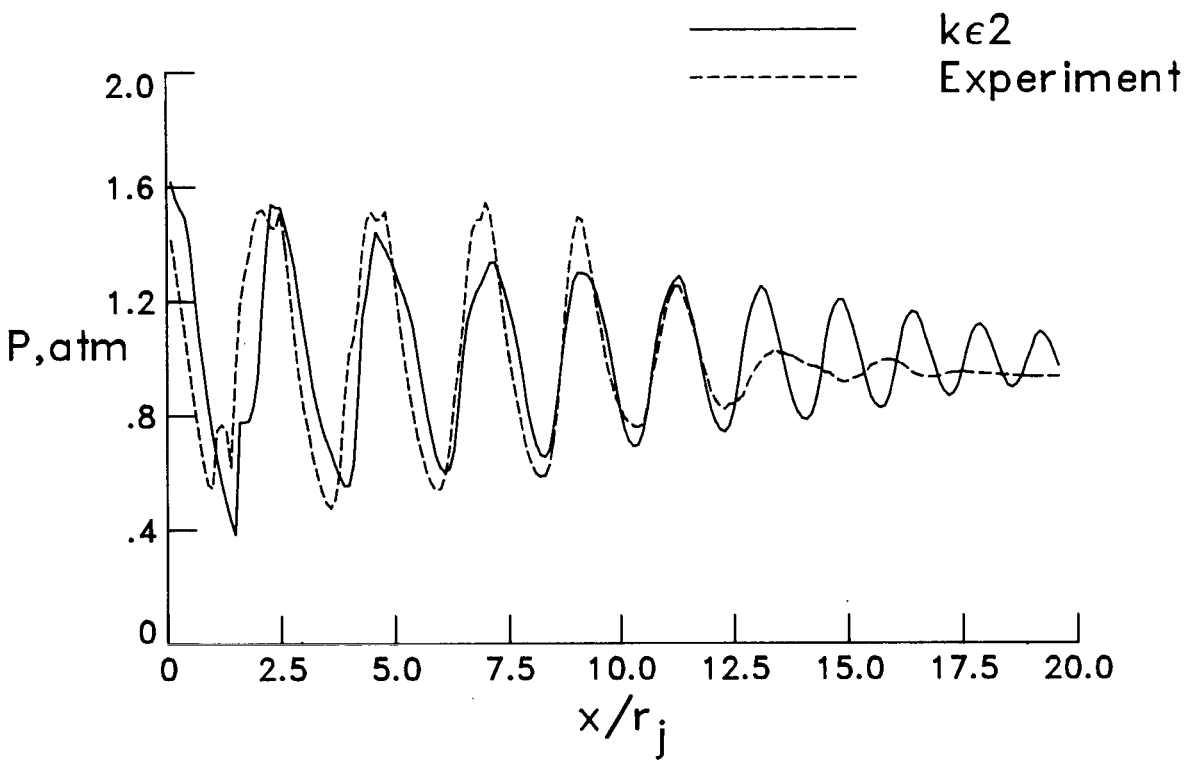

(b) Predicted and measured.

Figure 9. Concluded.

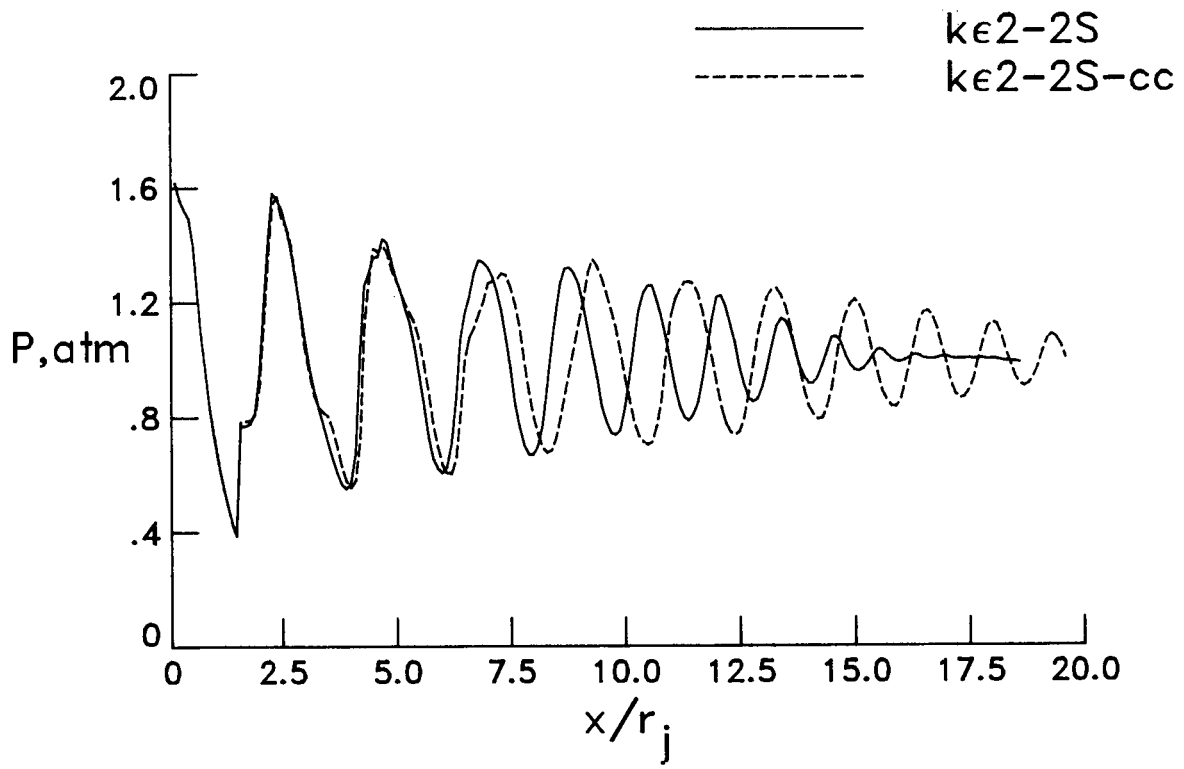

(a) Comparison between $k\varepsilon$2-2S and $k\varepsilon$2-2S-cc.

Figure 10. Effect of compressibility correction on two-scale $k\varepsilon$2-2S prediction for sonic jet.

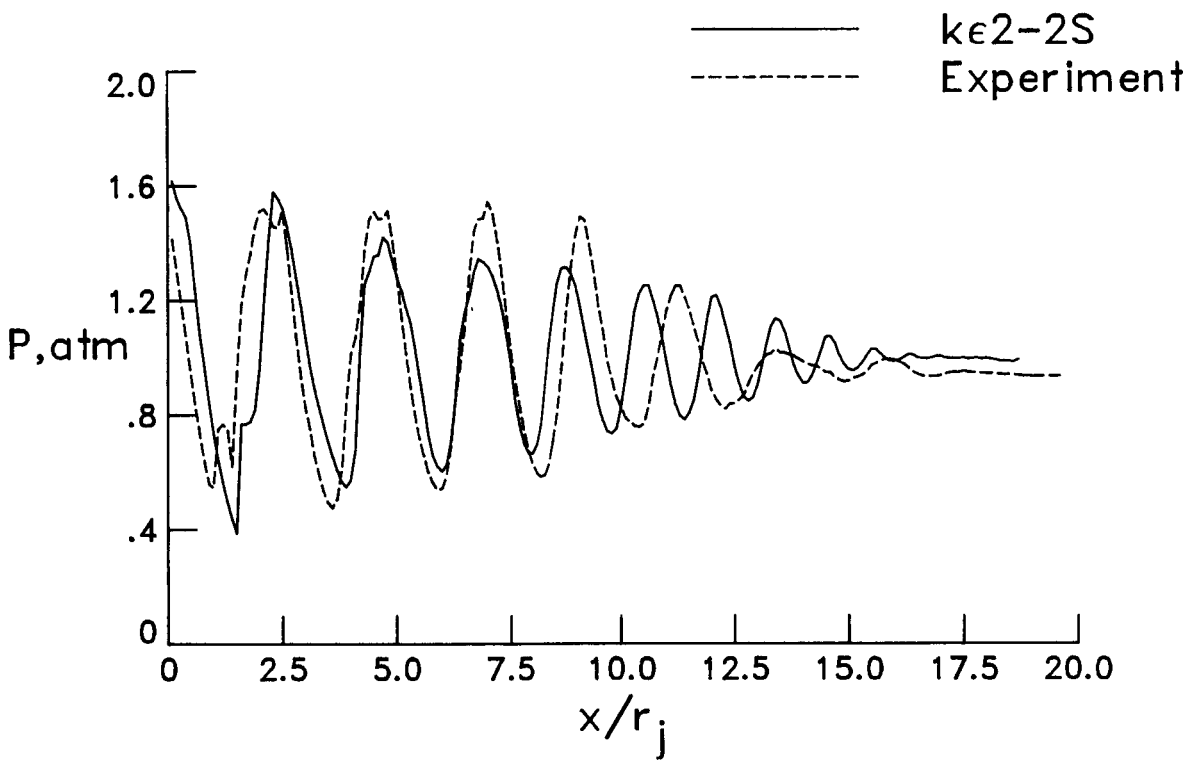

(b) Predicted and measured.

Figure 10. Concluded.

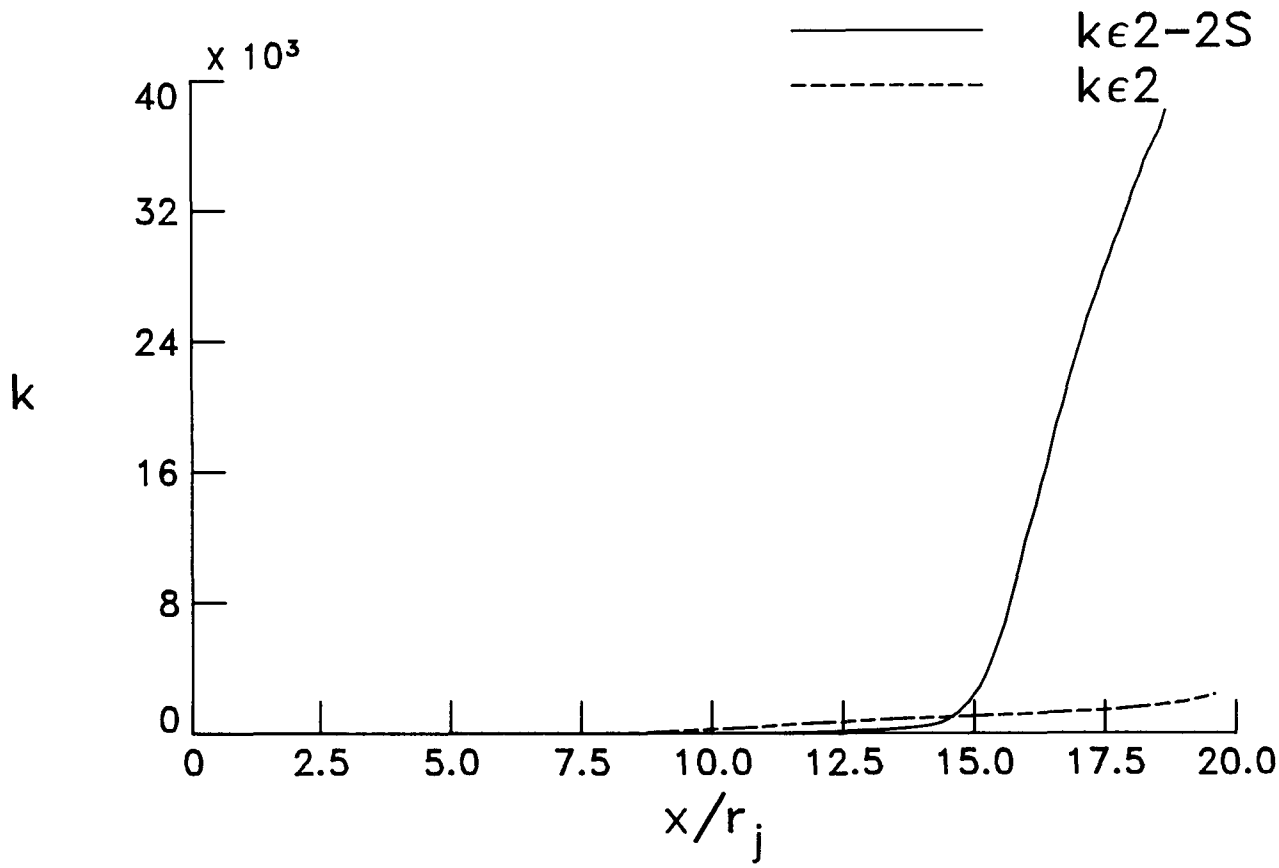

Figure 11. Comparison of total turbulent kinetic energy calculated using $k\varepsilon 2$ and $k\varepsilon$2-2S for sonic jet.

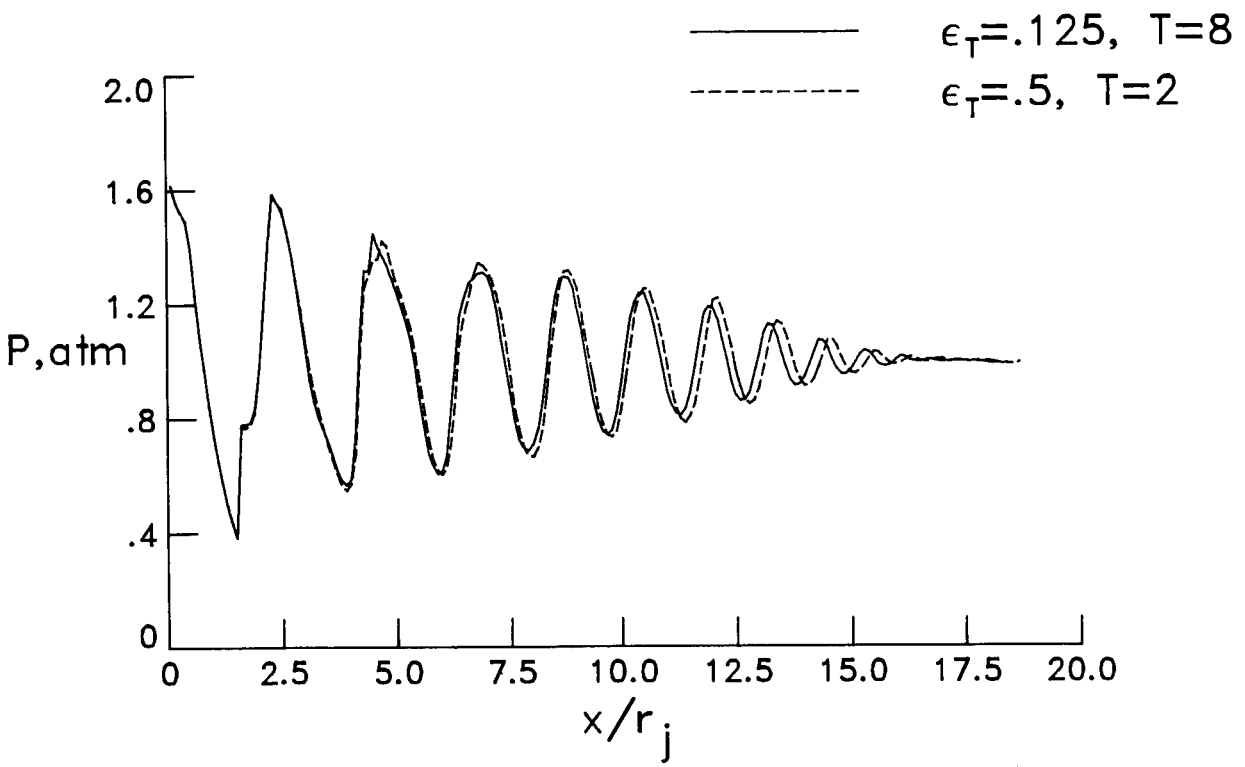

(a) Effect of initial dissipation ε_T (case 1).

Figure 12. Effect of initial conditions on predicted centerline pressures for sonic jet.

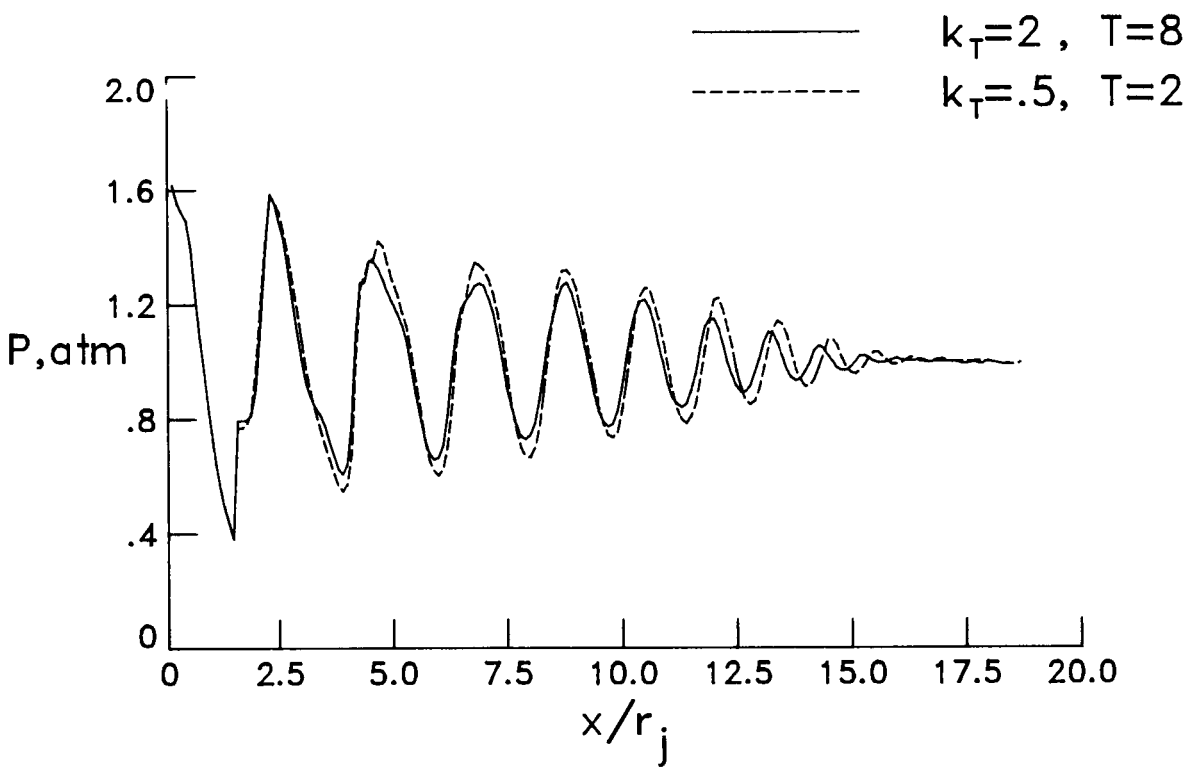

(b) Effect of initial kinetic energy k_T (case 2).

Figure 12. Concluded.

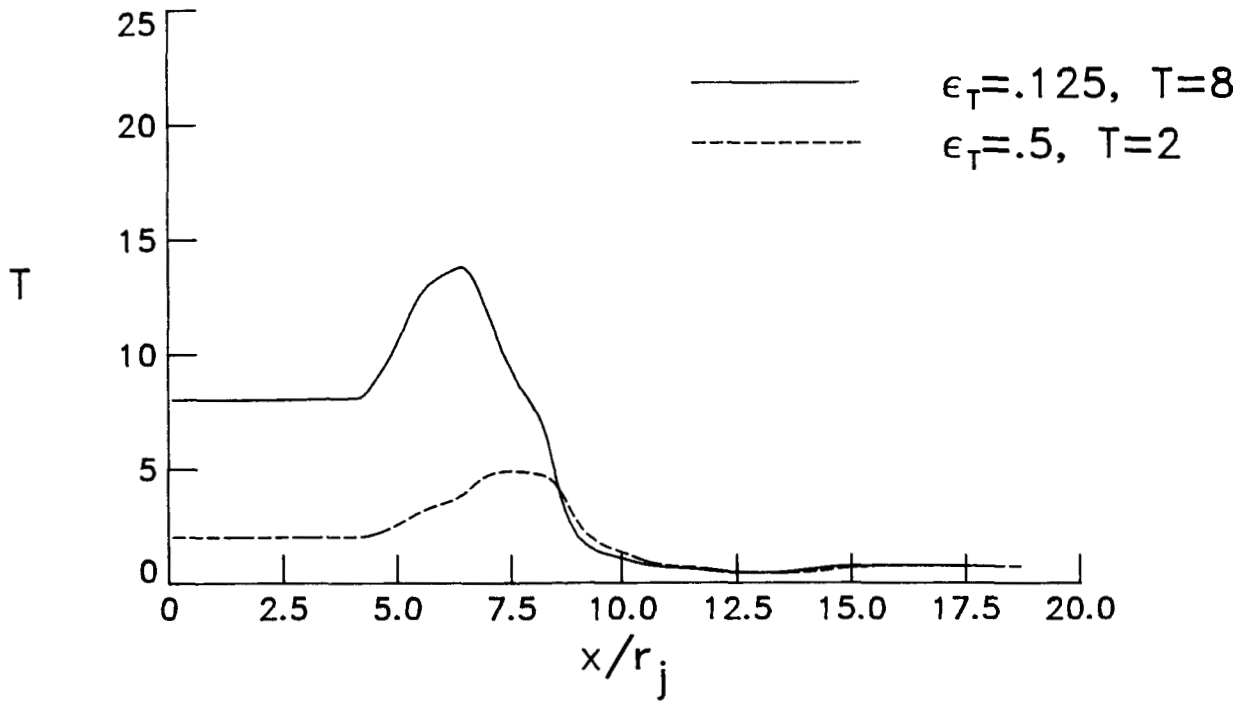

(a) Effect of initial dissipation ε_T (case 1).

Figure 13. Effect of initial conditions on predicted centerline time-scale ratio for sonic jet.

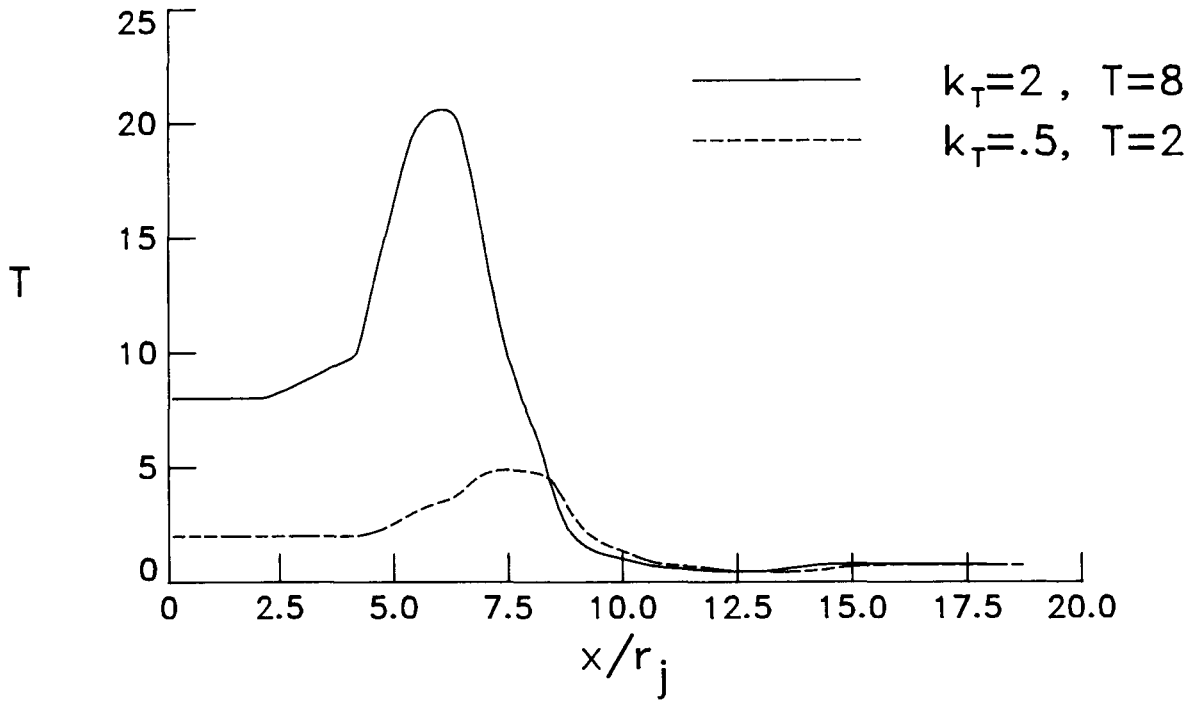

(b) Effect of kinetic energy k_T (case 2).

Figure 13. Concluded.

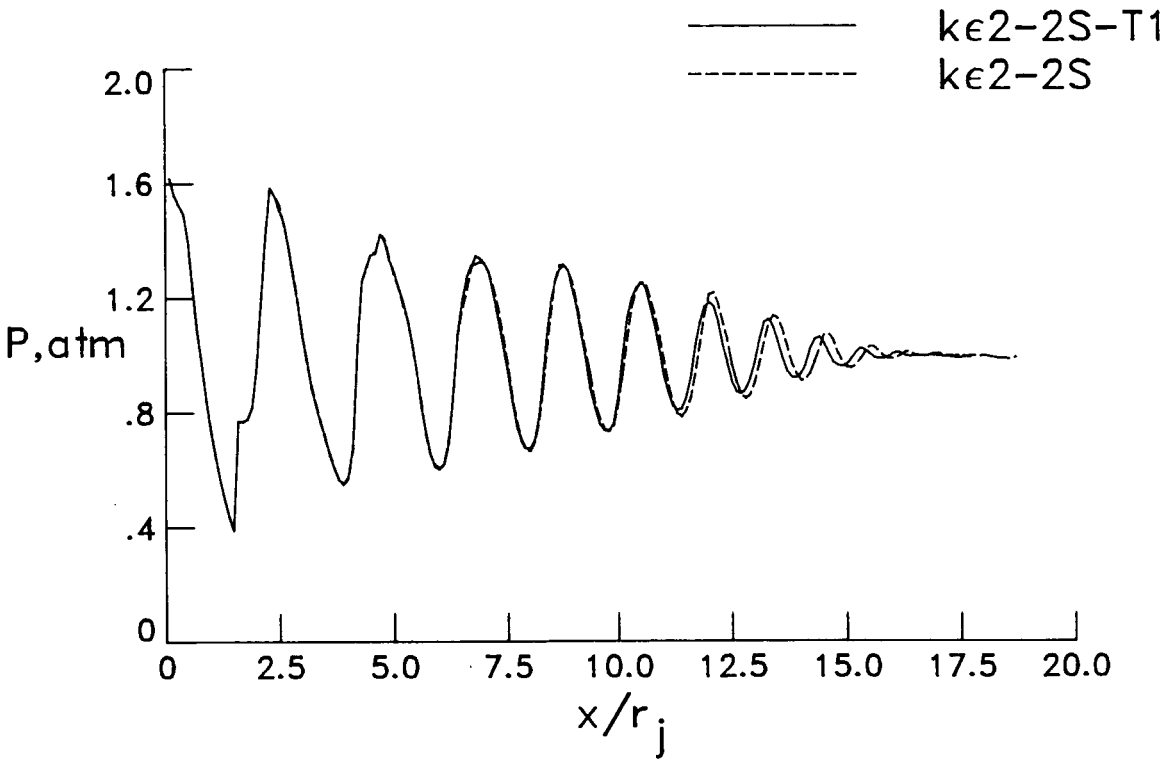

(a) Comparison between $k\varepsilon$2-2S-T1 and $k\varepsilon$2-2S.

Figure 14. Prediction of centerline pressures using modified two-scale model T1 for sonic jet.

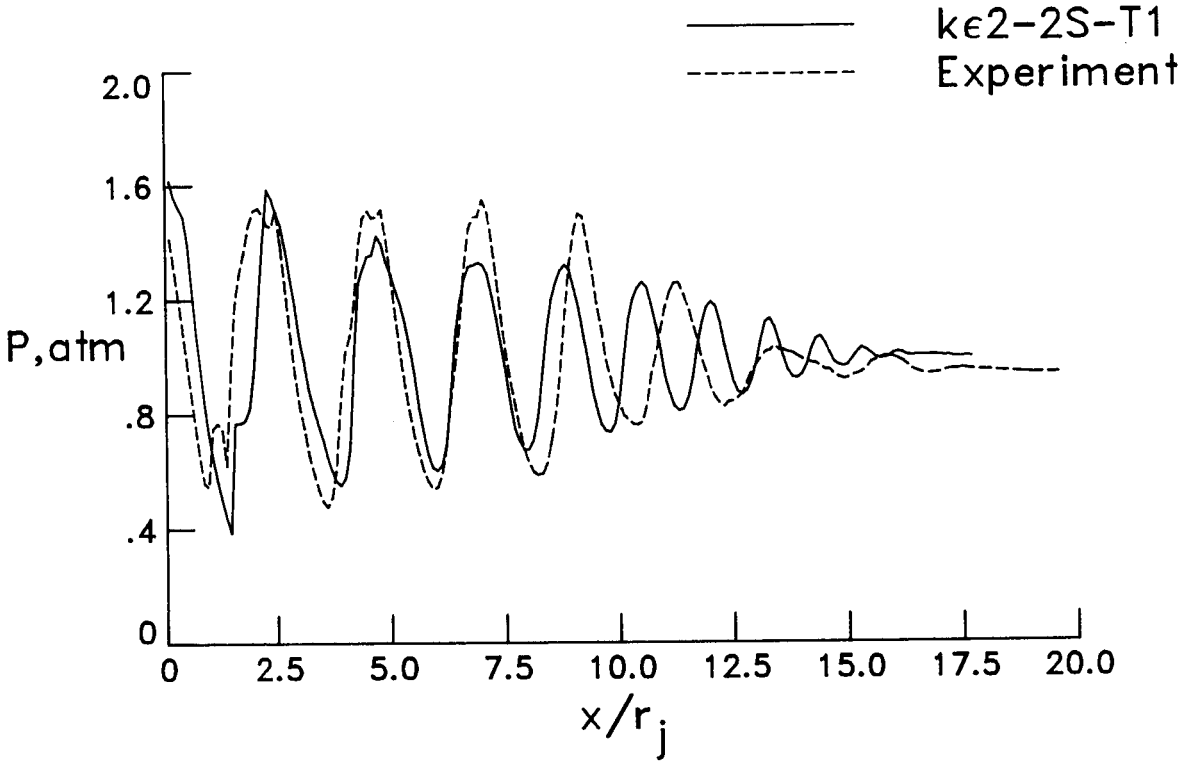

(b) Predicted and measured.

Figure 14. Concluded.

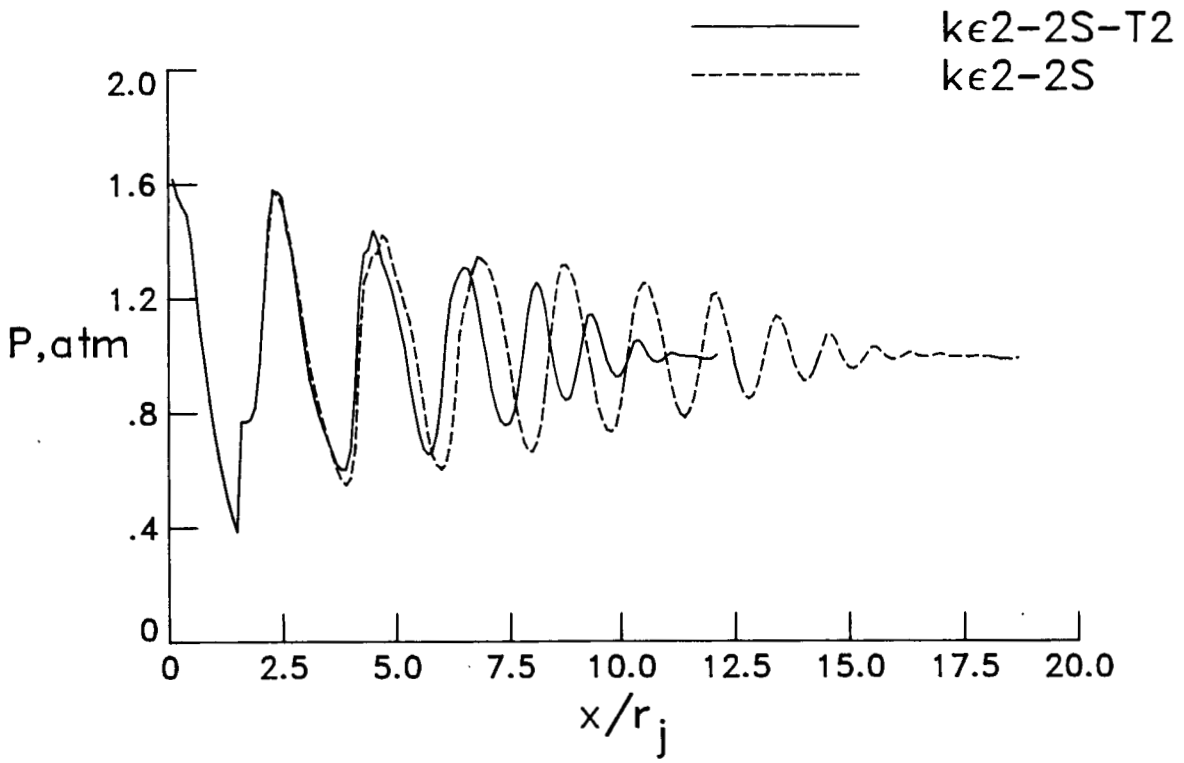

(a) Comparison between $k\varepsilon$2-2S-T2 and $k\varepsilon$2-2S.

Figure 15. Prediction of centerline pressures using modified time-scale model T2 for sonic jet.

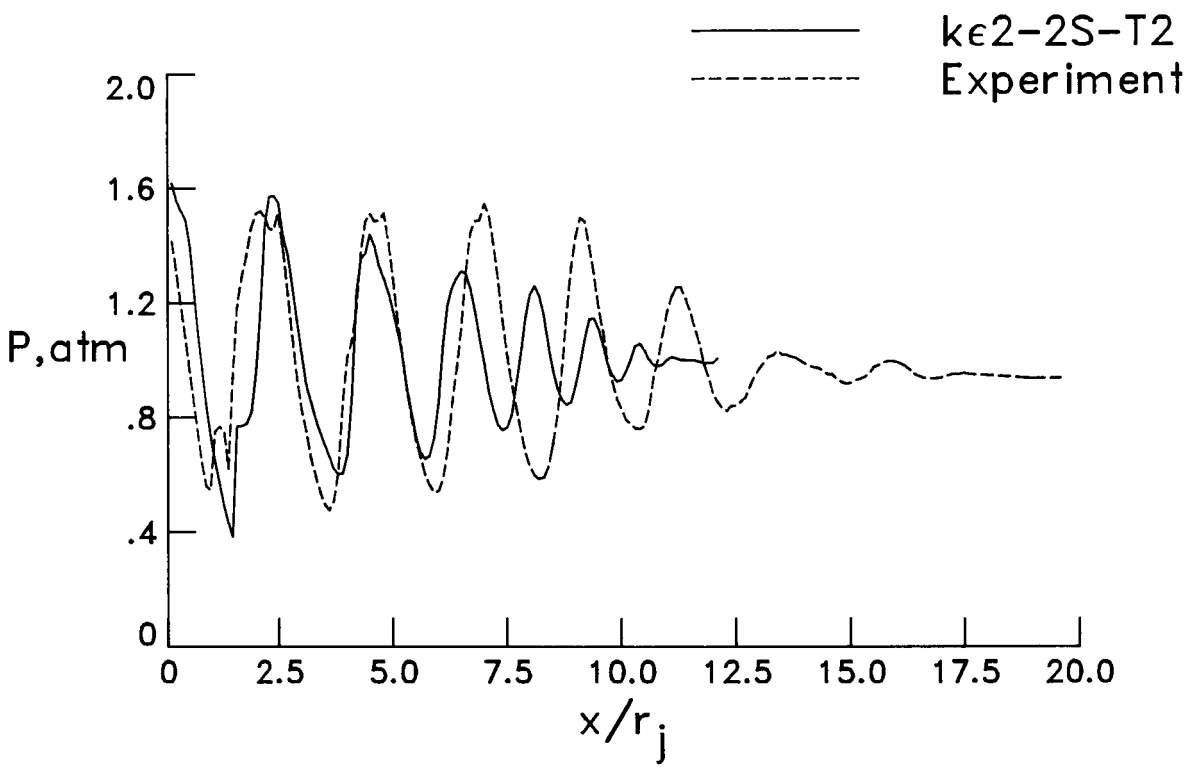

(b) Predicted and measured.

Figure 15. Concluded.

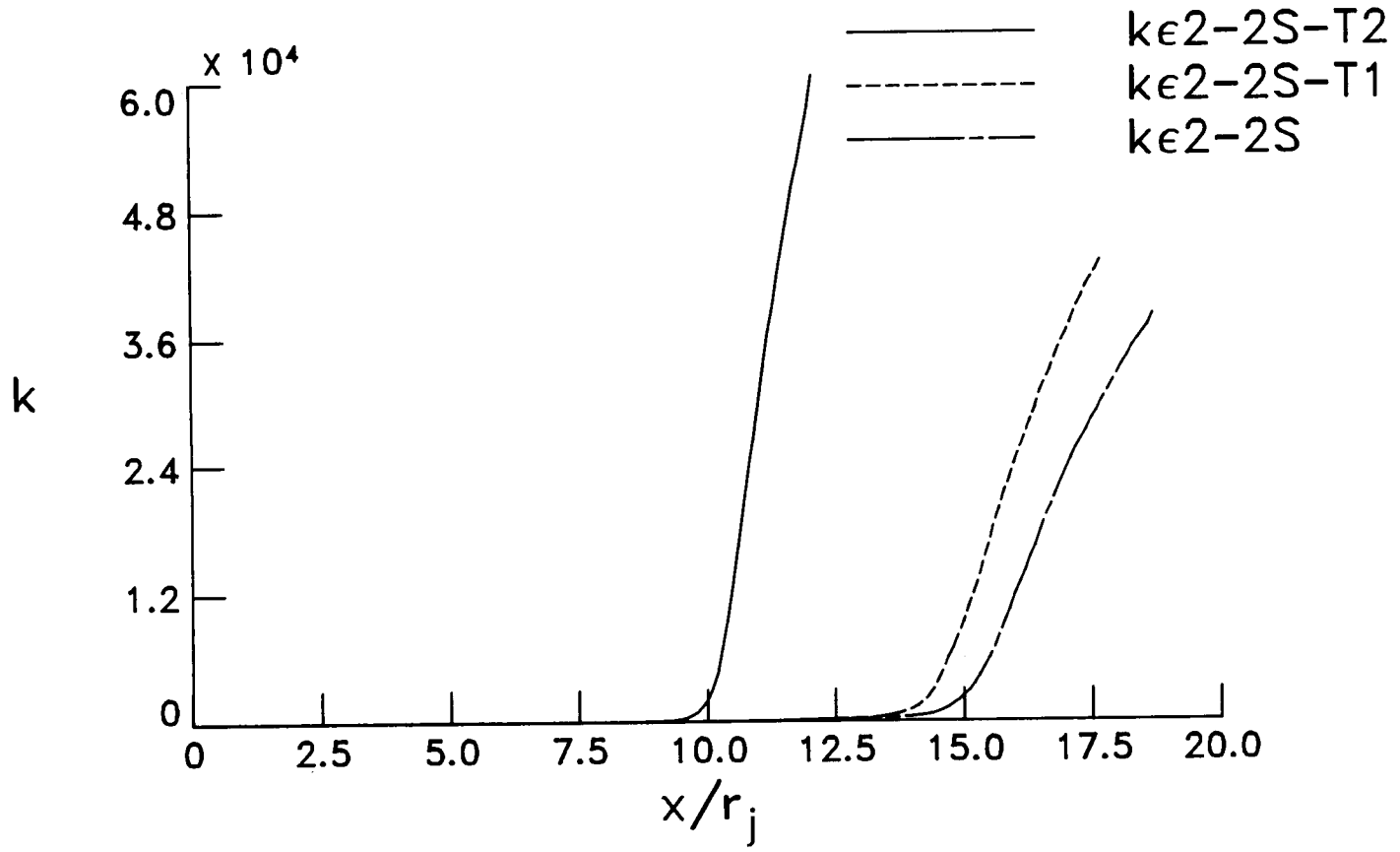

Figure 16. Comparison of calculated total kinetic energy for sonic jet using $k\varepsilon$2-2S, $k\varepsilon$2-2S-T1, and $k\varepsilon$2-2S-T2.

NASA
National Aeronautics and Space Administration

Report Documentation Page

1. Report No.	2. Government Accession No.	3. Recipient's Catalog No.
NASA TP-2707		

4. Title and Subtitle	5. Report Date
Multiscale Turbulence Effects in Supersonic Jets Exhausting Into Still Air	July 1987
	6. Performing Organization Code
7. Author(s)	8. Performing Organization Report No.
Khaled S. Abdol-Hamid and Richard G. Wilmoth	L-16258
9. Performing Organization Name and Address	10. Work Unit No.
NASA Langley Research Center Hampton, VA 23665-5225	505-62-91-01
	11. Contract or Grant No.
12. Sponsoring Agency Name and Address	13. Type of Report and Period Covered
National Aeronautics and Space Administration Washington, DC 20546-0001	Technical Paper
	14. Sponsoring Agency Code

15. Supplementary Notes

Khaled S. Abdol-Hamid: Analytical Services and Materials, Inc., Hampton, Virginia.
Richard G.Wilmoth: Langley Research Center, Hampton, Virginia.

16. Abstract

A modified version of the multiscale turbulence model of Hanjalic has been applied to the problem of supersonic jets exhausting into still air. In particular, the problem of shock-cell decay through turbulent interaction with the mixing layer has been studied for both mildly interacting and strongly resonant jet conditions. The modified Hanjalic model takes into account the nonequilibrium energy transfer between two different turbulent spectral scales. The turbulence model was incorporated into an existing shock-capturing, parabolized Navier-Stokes computational model in order to perform numerical experiments. The results show that the two-scale turbulence model provides significant improvement over one-scale models in the prediction of plume shock structure for underexpanded supersonic (Mach 2) and sonic (Mach 1) jets. For the supersonic jet, excellent agreement with experiment was obtained for the centerline shock-cell pressure decay up to 40 jet radii. For the sonic jet, the agreement with experiment was not as good, but the two-scale model still showed significant improvement over the one-scale model. It is shown that by relating some of the coefficients in the turbulent-transport equations to the relative time scale for transfer of energy between scales, the two-scale model can provide predictions that bound the measured shock-cell decay rate for the sonic jet.

17. Key Words (Suggested by Authors(s))	18. Distribution Statement
Turbulence models Multiscale effects Parabolized Navier-Stokes solutions Supersonic jets Shock-cell decay Jet noise	Unclassified—Unlimited Subject Category 34

19. Security Classif.(of this report)	20. Security Classif.(of this page)	21. No. of Pages	22. Price
Unclassified	Unclassified	36	A03

NASA FORM 1626 OCT 86 NASA-Langley, 1987
For sale by the National Technical Information Service, Springfield, Virginia 22161-2171